Journal of the Serbian Chemical Society
JSCS-info@shd.org.rs • www.shd.org.rs/JSCS

ACCEPTED MANUSCRIPT

Please cite this article as K. K. Yadav, A. Kumar, S. Begam, K. Nurjamal, A. Kumar, G. Brahmachari, N. Misra, *J. Serb. Chem. Soc.* (2019)
https://doi.org/10.2298/JSC181228102Y

J. Serb. Chem. Soc. 84 (0) 1-14 (2019)
JSCS–7702

UDC
Original scientific paper

Spectroscopic (FTIR, UV-Vis and NMR), theoretical investigation and molecular docking of substituted 1,8-dioxodecahydroacridine derivatives

KRISHNA KANT YADAV[1], ABHISHEK KUMAR[1], SANCHARI BEGAM[2], KHONDEKAR NURJAMAL[2], AMARENDRA KUMAR[1,*], GOUTAM BRAHMACHARI[2] and NEERAJ MISRA[1]

[1]*Department of Physics, University of Lucknow, Lucknow-226007, India;*
[2]*Laboratory of Natural Products & Organic Synthesis, Department of Chemistry, Visva-Bharati (a Central University), Santiniketan-731 235, West Bengal, India*

(Received 28 December 2018; revised 6 September 2019; accepted 16 September 2019)

Abstract: Recently, substituted 1, 8-dioxodecahydroacridine derivatives have been investigated and found to possess a wide variety of biological and pharmacological activities. Two of these biologically relevant *N*-heterocyclic scaffolds 2-(9-(4-methoxyphenyl)-3,3,6,6-*tetra*methyl-1,8-dioxo-1,2,3,4,5,6,7,8-*octa*hydroacridin-10(9*H*)--yl)succinic acid (MTDOSA) and 2-(3,3,6,6-*tetra*-methyl-9-(4-nitrophenyl)-1,8--dioxo-1,2,3,4,5,6,7,8-*octa*hydroacridin-10(9*H*)-yl)succinic acid (NTDOSA) have been studied in ground and first excited state using DFT method employingB3LYP/6-311++G(d,p) level of theory. Quantum chemical calculations of geometrical structure and vibrational wavenumbers of MTDOSA andNTDOSA were carried out using DFT method. The experimental FT-IR spectra of the compounds are recorded in the range 4000-400 cm^{-1} and comprehensively interpreted on the basis ofpotential energy distribution. The global reactivity descriptors are calculated and discussed. Moreover, ^{1}H and ^{13}C NMR spectra have been calculated by using the gauge independent atomic orbital method and compared with experimental spectra. The docking studies reveal that the compounds MTDOSA and NTDOSA have strong binding affinity toward target protein 5KLH. Thus, the compounds have a possible use as an antileishmanial drug.

Keywords: quantum chemical study; spectroscopy; global reactivity descriptors; antileishmanial drug

INTRODUCTION

Diversely substituted 1,8-dioxodecahydroacridine derivatives have been studied for their wide range of notable pharmacological properties including antimalarial, antitumor, antiprion, anti-Alzheimer's, antimicrobial, antileishmanial and antitrypanosomal[1-3] in last decade. Positive ion tropic effects have been exhibited by acridines[4] and its derivatives such as 1,8- dioxodecahydroacridines are also

*Corresponding author: akgkp25@yahoo.co.in
https://doi.org/10.2298/JSC181228102Y

recognized as laser dyes.[5] Having wide range of applicability, various synthetic procedures have been adapted to generate these biologically important compounds and their derivatives.[6,7] G. Brahmachari *et. al.*[8] recently reported a simple and convenient, eco-friendly, low-cost and practical protocol for the synthesis of a new series of diversely substituted 1,8-dioxodecahydroacridines, particularly bearing various amino acids as part of the building block. Keeping diverse biological and pharmacological properties of substituted 1,8-dioxodecahydroacridine derivatives in mind, herein we are presenting a detailed comparative study of geometric and electronic structure of 2-(9-(4-methoxyphenyl)-3,3,6,6-*tetra*methyl-1,8-dioxo-1,2,3,4,5,6,7,8-*octa*hydroacridin-10(9*H*)-yl)succinic acid (MTDOSA) and 2-(3,3,6,6-*tetra*methyl-9-(4-nitrophenyl)-1,8-dioxo-1,2,3,4,5,6,7,8-*octa*hydroacridin-10(9*H*)-yl)succinic acid(NTDOSA) in ground and first excited state The experimental spectral data (FT-IR, UV and NMR) of MTDOSA and NTDOSA are compared with the data calculated using theoretical (DFT/B3LYP) method. The molecular properties such as dipole moment, molecular electrostatic potential surfaces and frontier orbital band gap energies have been calculated for the better understanding of the properties of both the compounds. Since the compounds under consideration are substituted derivatives of a biologically and pharmacologically active moiety, global reactivity descriptors like chemical potential, electronegativity, hardness, softness and electrophilicity index have been calculated and used to predict the reactivity of the molecules.

EXPERIMENTAL DETAILS

The FT-IR spectrum of title molecules were recorded between 4000-400 cm^{-1} on a Shimadzu (FT-IR 8400S) FT-IR spectrophotometer using KBr disc. UV-Visible spectra for MTDOSA and NTDOSA were measured on a Shimadzu UV-1800 spectrophotometer with 1 cm quartz cell optical path length using MeOH as solvent with their respective concentration of 2.02×10^{-4} and 1.96×10^{-4} mol L^{-1}. Their ^{1}H and ^{13}C NMR spectra were obtained at 400 and 100 MHz, respectively, using Bruker DRX-400 spectrometer and DMSO-d_6 as the solvents. Solvents were purchased from Sigma Aldrich.

General procedure for the synthesis of substituted 1,8-dioxoacridines 4a and 4b

The title compounds were synthesized following the methodology previously published by us (Scheme 1).[8] Dimedone (**1**; 1 mmol), aspartic acid (**2**; 1 mmol), $Bi(NO_3)_3.5H_2O$ (10 mol%; 49 mg) and 4 mL dry ethanol were transferred to an oven-dried sealed-tube in a sequential manner at ambient conditions, and the reaction mixture was then stirred vigorously for about 2 h. After then another part of dimedone (**1**; 1 mmol) and 4-methoxybenzaldehyde (**3a**, 1 mmol)/ 4-nitrobenzaldehyde (**3b**, 1 mmol) was added to the stirred reaction mixture, and the stirring was continued up to next 14 h under same reaction conditions. The progress of the reaction was monitored by TLC. On completion of the reaction, a solid mass precipitated out which was filtered off, followed by purification of the crude product by recrystallization from ethanol to furnish pure product **4a/4b** (Fig. 1). The structure for each of the products was confirmed by analytical as well as spectral studies including FT-IR, ^{1}H NMR, ^{13}C NMR and DEPT-135. Characterization data of the synthesized compounds 4a and 4b are given in supplementary information.

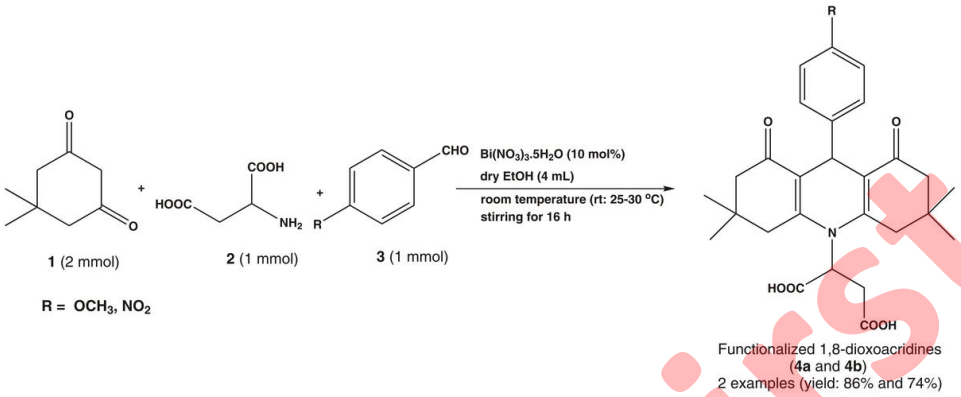

Scheme 1. Bismuth nitrate-catalyzedone-pot synthesis of substituted 1,8-dioxoacridines (**4a**/**4b**) at ambient conditions

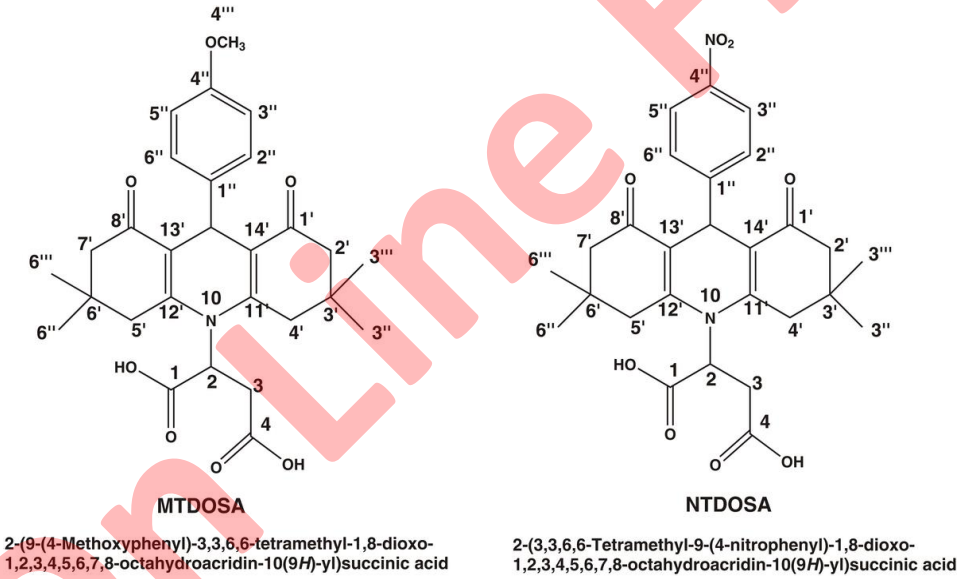

Fig. 1: Chemical structures of MTDOSA and NTDOSA with atom numeration

COMPUTATIONAL DETAIL

All computations herein were executed using the GAUSSIAN-09 program package.[9] B3LYPof DFT and 6-311++G (d, p) basis setwas used throughout the calculations. The vibrational unscaled wavenumbers are calculated and scaled down by the appropriate factor.[10,11] The vibrational wavenumber assignments have been carried out by the corresponding potential energy distributions (PEDs) and the PEDs are computed from the VEDA 4 program[12]. TD-DFT calculations were performed in conjugation with IEFPCM model for solvent effect in methanol. ^{1}H and ^{13}C NMR chemical shifts of title compound were obtained using including atomic orbital (GIAO) methodin DMSO at DFT/B3LYP method with 6-311++G(d,p) basis set.

RESULTS AND DISCUSSION

Molecular geometry

The geometry optimization for both the molecules has been achieved by energy minimization, using DFT at the B3LYP level with 6-311++G(d,p) basis set. Optimized geometry of the molecules is further ensured to be located at the local true minima on potential energy surface, because calculated vibrational spectra contain no imaginary wavenumber. The calculated optimized geometrical parameters (bond lengths, bond angles and dihedral angles) of the MTDOSA and NTDOSA molecules are listed in Tables SI and SII respectively, and the optimized molecular structures thus obtained along with the numbering scheme of the atoms are depicted in Fig. 2. In the six-membered rings (R1, R2 and R3) of molecules MTDOSA/NTDOSA, all the C–C bonds, N-C bond and C-H bond lengths are in full agreement with those reported in literature.[13] In both the molecules C=O bond lengths are equal to 1.221 Å, close to the standard C=O bond length (1.220 Å)[13,14].

In both the molecules (MTDOSA /NTDOSA), the fusedrings R2, R3 and R4 are showing some non-planarity as evident from the dihedrals involved (C1-C6-C5-C10=173.02^{o} /174.38^{o} and C10-C9-C14-C13=172.14^{o} /173.41^{o}). The dihedrals C5-C10-C17-C12 (41.44/41.97) and C9-C10-C17-C18 (96.70/97.11) show non-planarity of ring R1 with ring R3.

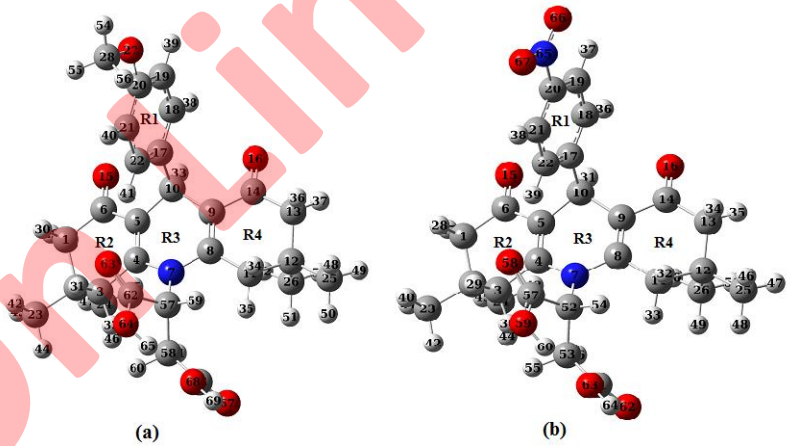

Fig. 2: The optimized geometric structure of (a) MTDOSA (b) NTDOSA molecule

Vibrational analysis and FTIR spectrum

The theoretical vibrational analysis of both the molecules were performed by using B3LYP level with 6-311++G (d,p) basis set. The experimental and calculated vibrational wavenumbers of MTDOSA and NTDOSA along with their PED are given in Tables SIII and SIV respectively. The calculated harmonic wavenumbers are generally slightly higher than that of their experimental

counterpart. So, proper scaling factors[10, 11] are employed to have a better agreement with the experimental wavenumbers. In the present study, vibrational wavenumbers calculated at B3LYP/6-311++G (d,p) level have been scaled by 0.967. The calculated IR spectrum of both the molecules agree well with the recorded FTIR spectra using Shimadzu (FTIR 8400S) spectrometer in the region 4000-400 cm^{-1} using samples in KBr disc. The experimental FT-IR and theoretical IR spectra of MTDOSA and NTDOSA have been shown in Fig. 3. This is to be mentioned herein that the FT-IR absorption peaks around 2360 cm^{-1} (experimental error and not characteristics of the chemical structures of the title molecules) recorded in both the spectra are due to atmospheric carbon dioxide encapsulated within the pores of the walls of KBr disc during sample preparation.

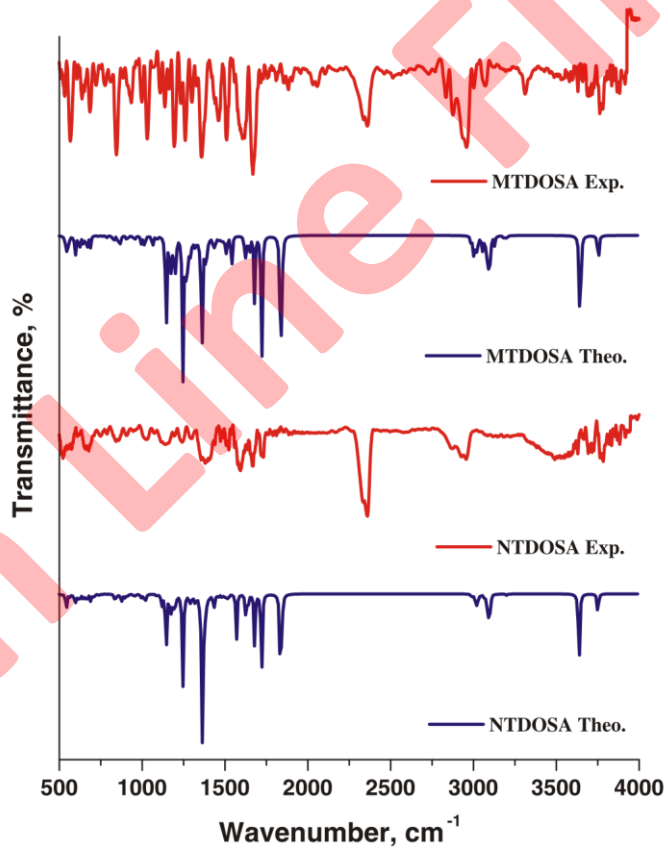

Fig. 3. The calculated IR and experimental FTIR spectra of MTDOSA and NTDOSA molecule

O-H vibrations

Generally, the O-H stretching vibrations are found to be in the region around 3500 cm^{-1}.[15] In case of MTDOSA/NTDOSA the calculated stretching modes are

found at 3629/3627 and 3523/3517 cm^{-1}. The O–H in-plane bending vibration, in general lies in the region 1150–1250 cm^{-1}.[15] In the present study of molecule MTDOSA/NTDOSA, the O–H in-plane bending vibration appears as a weak band in both the molecule in the range 1275-1316/1253-1316 cm^{-1}.

Ring vibrations

In case of aromatic compounds multiple weak bands are generally observed in the range 3100–3000 cm^{-1}.[16] These bands are due to aromatic C–H stretching vibrations. In the present study, in case of MTDOSA and NTDOSA, both having three aromatic rings fused with each other and one phenyl ring show very weak bands in this region of the FTIR spectra. The symmetric and asymmetric C–H stretching modes of MTDOSA/NTDOSA are calculated at 3097/3115, 3090/3094, 3083/3093, 3001/3002, 2981/2983 and 2960/2962 cm^{-1} are assigned well with FTIR spectra.

C=O vibration

In IR spectra the appearance of a band around 1700 cm^{-1}shows the presence of carbonyl group and is due to the C=O stretching. In the present study the asymmetric and symmetric stretching modes of C=O groups calculated at higher wave-number (1785/1784 cm^{-1}) and the one at slightly lower wavenumber (1660/1659 cm^{-1}) of MTDOSA/NTDOSA.

CH_3 vibrations

Both the compounds (MTDOSA/NTDOSA) have four methyl groups attached with the aromatic ring (R2 and R4). The anti-symmetric and symmetric C–H stretching mode of the CH_3 group is expected around 2980 and 2870 cm^{-1} respectively. The asymmetric C-H stretching vibrational modes of CH_3 are calculated at 2987, 2983, 2975, 2974 cm^{-1} and 2997, 2989, 2988, 2984 cm^{-1} for MTDOSA and NTDOSA molecules respectively. Symmetric CH_3 stretching modes for MTDOSA and NTDOSA molecules are calculated at 2926, 2923 and 2978, 2975 cm^{-1} respectively. The bending mode of vibrations of methyl group appears within the region 1465–1440 cm^{-1}. In the present investigation the wavenumbers corresponding to CH_3 bending vibration are ranges from 1464 to 1456 cm^{-1} in both the molecules.

UV-Vis analysis

Ultraviolet spectral analyses of MTDOSA and NTDOSA molecules have been studied by experimental and TD-DFT/B3LYP/6-311++G (d, p) method. The electronic spectra have been recorded in methanol at room temperature. The calculated absorption wavelengths, nm, oscillator strengths (*f*) and vertical excitation energies (*E*) in methanol solution phase were carried out and compared with experimental values (Tables SV and SVI). The comparative experimental and theoretical UV-Vis spectrum of MTDOSA and NTDOSA has been given in Fig. 4.

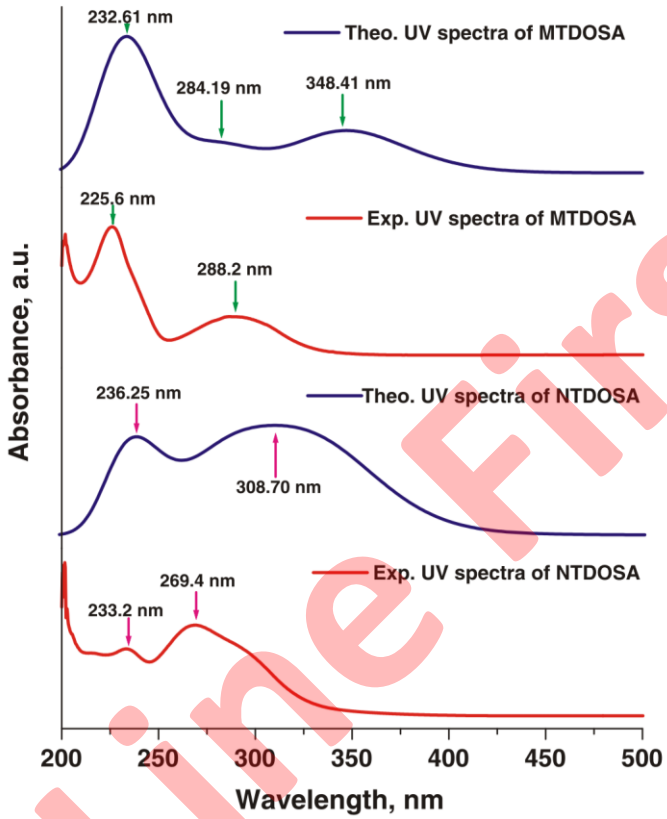

Fig. 4. Recorded and calculated UV-spectra of MTDOSA and NTDOSA in methanol solvent

One can note that there are two intense peaks observed at 288.2 nm and 225.6 nm in experimental spectra of MTDOSA in methanol which are assigned by peaks in calculated spectra at 284.19 and 232.61 nm respectively. Another peak at 348.41 nm has also been observed in theoretical UV Spectra. These absorption maxima at 284.19, 232.61 and 348.41 nm result due to electronic transition from HOMO→LUMO+1, HOMO-4→LUMO+1 and HOMO-1→LUMO. In the case of NTDOSA, calculated absorption maxima at 236.25 nm corresponds to the electronic transition HOMO→LUMO+7 and is in good agreement with the experimental absorption peak at 233.2 nm.

NMR analysis

Nuclear magnetic resonance (NMR) spectroscopy provides detailed information about the electronic structure and an important tool to probe the surroundings of a nucleus. Carbon and hydrogen shielding tensors of MTDOSA and NTDOSA molecules are studied using both experimental and theoretical techniques. The experimental ^{1}H and ^{13}C NMR spectra of MTDOSA and NTDOSA are

given in Fig. S1 to Fig. S8. ^{1}H and ^{13}C NMR chemical shifts of the title molecules were calculated with the optimized molecular structure atDFT-B3LYP/6-311++G (d,p) level using the GIAO method with TMS as a reference. The values of experimental chemical shift along with calculated chemical shifts of molecules under consideration are listed in supplementary tables (Tables SVII and SVIII).

Generally, the aromatic carbon shows chemical shift values from 100 to 150 ppm in ^{13}C NMR spectrum. The chemical shifts of carbon atoms of ring (R1) in MTDOSA were calculated in the range 114.61-167.59 ppm with experimental recorded value from 129.40 to 158.06 ppm in DMSO. This is due to presence of electron-donating group MeO which increased shielding in *ortho* positions. Due to the presence of electron with drawing group NO_2 which also increase the shielding, the molecule NTDOSA show the chemical shift of carbon in range 130.07-164.77 ppm, which is in good agreement experimental value ranges from 107.60 - 144.22 ppm increase in shielding by presence of electron.

In the ring R2 and R4 chemical shift of ^{13}C NMR vary in the range 42.68-205.96 / 42.42-206.23 ppm and experimentally recorded between 31.05-196.62 / 39.38-182.51ppm of MTDOSA/ NTDOSA. The C6 and C14 atoms have larger chemical shifts (205.96 / 205.92 and 205.93 / 206.23 ppm) than the other ring carbon atoms, due to de-shielding effect of electronegative oxygen atom. Due to the presence of electronegative nitrogen atoms in ring R3, the C4 and C8 atom get de-shielded hence correspond to nuclear magnetic resonances of higher frequencies. The carbon atomsC62, C66 in MTDOSA and C53, C57 in NTDOSA in carboxylic group get de-shielded due to the presence of two electronegative oxygen atoms hence shows chemical shift at higher value.

^{1}H NMR chemical shift of MTDOSA / NTDOSA show the presence of singlet in the range 0.81-1.36/0.82-1.36 ppm for protons of methyl group attached to the ring and experimental chemical shifts of ^{1}H NMR spectrum of these protons in DMSO solvent are in range of 0.97-1.08 / 1.83-2.25 ppm. The calculated doublet chemical shift of MTDOSA / NTDOSA ranges from 6.90-8.12 / 8.10-8.48 ppm corresponding to proton attached with ring R1. The ^{1}H NMR chemical shift of proton attached with ring R2 and R4 show presence of multiplet band in the range 1.86-2.95 / 1.91-2.91 ppm of MTDOSA / NTDOSA. A singlet at δ 5.35/5.50 ppm corresponds to protons directly attached to R3 of MTDOSA / NTDOSA. In the molecule MTDOSA a singlet is obtained in the range 3.76-4.11 ppm corresponds to protons of methyl group directly attached to the oxygen attached with R1.

Electronic parameters

Frontier molecular orbitals, namely highest occupied molecular orbital (HOMO) and lowest unoccupied molecular orbital (LUMO) determine the way the molecule interacts with other species. The energy difference between HOMO and LUMO can be used to predict the chemical reactivity and kinetic stability of

a molecule. A molecule with a small frontier orbital gap indicates its Polarizable nature and is generally associated with a high chemical reactivity, low kinetic stability and such a molecule is termed as soft molecule. In the present DFT study, the frontier orbital gaps in case of MTDOSA and NTDOSA are 3.899 and 4.012 eV, respectively *i.e.* the frontier orbital gap in MTDOSA is 0.113 eV lower than NTDOSA. The 3D plots of HOMO and LUMO frontier molecular orbitals for both molecules are shown in Fig. S3. In the compound MTDOSA, HOMO is found to be distributed mostly over the entire Compound except the phenyl ring (R1) and methoxy group while the LUMO is mostly contributed by methoxy phenyl ring with a small involvement of entire fused heterocyclic ring but in case of NTDOSA the contribution of HOMO is over the nitro phenyl ring (R1) and a little involvement of all fused heterocyclic rings whereas LUMO is distributed over the whole molecule except nitro phenyl ring.

Electronic chemical potential (μ), absolute hardness (η), and global electrophilicity index (ω)[17,18] are the descriptors of molecular stability and reactivity. These universal concepts may be defined using DFT. According to Parr and Pearson[19] the electronic chemical potential μ (which is equal to the negative of the electronegativity of atoms and molecules) was defined as

$$\mu = -1/2\ (I + A) \tag{1}$$

Where I is the vertical ionization energy and A stands for the vertical electron affinity. Absolute hardness can be shown to be[17-22]:

$$\eta = I - A \tag{2}$$

Furthermore, the global electrophilicity index ω was introduced by Parr[17,23,24] and may be obtained using the electronic chemical potential μ and the absolute hardness η:

$$\omega = \frac{\mu^2}{2\eta} \tag{3}$$

The parameter ω defines the capability of a species to accept electrons. Thus, the low value of ω has been associated with a good nucleophile while a high value of it characterizes a good electrophile. This new reactivity quantity has been manifested recently in explaining the toxicity of various pollutants in terms of their reactivity and site selectivity[25]. The calculated values of the global reactivity parameters for the MTDOSA and NTDOSA molecules have been reported in Table 1. The substituted acridine derivative MTDOSA contains substituent donor methoxyphenyl that increases the energy of the HOMO and of the LUMO while NTDOSA contain substituent acceptor nitrophenyl decreases the energy of the HOMO and LUMO. The energy gap in MTDOSA (3.899 eV) is higher than NTDOSA (4.012 eV) reveals MTDOSA is more reactive in comparison to NTDOSA. The high value of chemical potential (-3.7149 eV) and

low value of electrophilicity index (1.7694 eV) for MTDOSA characterizes its electrophilic behavior while compound NTDOSA having lower value of chemical potential (-4.4405 eV) and higher value of electrophilicity index (2.4567 eV) makes its character nucleophilic.

Table I. Electronic parameters of MTDOSA and NTDOSA at B3LYP/6311++ G(d,p)

Reactivity descriptors	DFT/B3LYP/6311++G(d,p)	
	MTDOSA	NTDOSA
I / eV	5.6647	6.4470
A / eV	1.7651	2.4348
H / eV	3.8996	4.013
M / eV	-3.7149	-4.4405
ω / eV	1.7694	2.4567

Molecular electrostatic potential

The molecular electrostatic potential (MEP) and electronic density are related to each other and the MEP yields information on the molecular regions, which are preferred or avoided by an electrophile or nucleophile. MEP is a very useful parameter for determining reactive sites in the molecular system[26].The electrostatic potential increases by different colors in the order of red < orange < yellow < green < blue. The maximum negative region indicated by red color represents the site for electrophilic attack while the regions of nucleophilic attack indicated by blue color indicate maximum positive region represent[27-28]. MEPs for both the molecules were plotted using B3LYP/6-311++G(d,p) level for the optimized geometry, to predict the reactive sites for electrophilic and nucleophilic shown in Fig. S 10. From the MEP map of MTDOSA it can be seen that the region of negative potential is over the oxygen atom and the region having positive potential is over the hydrogen atoms of the fused rings. In case of NTDOSA the most negative potential region is hovering over nitro group and all the oxygen.

Molecular docking

The molecular docking reveals about the process by which a drug (molecule) and a receptor fit together and dock to each other well and the molecule binding to a receptor inhibits its function and thus acts effectively as a drug. The docking was done by Swiss Dock[29] which avoids sampling bias and provides a way of docking over whole protein without specifying the region of the protein as a bonding pocket. The resulting output clusters obtained after each run and the result for both the compounds shows that cluster 0 is having the best full fitness (FF) score. The more favorable binding site between a ligand and its receptor is signified by highest negative FF score. On account of antileishmanial activities shown by substituted 1,8-dioxodecahydroacridine derivative, the docking studies have been performed on the title compounds, MTDOSA and NTDOSA with Trypnosoma Brucei pro-cyclic specific surface antigen-2(TbPSSA-2) (PDB ID:

5KLH)[30], the reason for the vector-borne diseases of humans and livestock in sub-Saharan Africa. The FF score obtained for protein targets clearly shows that the molecule MTDOSA is bonded with the target protein with one hydrogen bond 2.583 Å (FF score: -1466.9 kcal/mol and binding affinity Δ*G*: -7.57 kcal/mol) and NTDOSA are effectively bonded with 5KLH target with four hydrogen bond at 2.030, 2.036, 2.295 and 2.355 Å respectively (FF score: -1459.1 kcal/mol and binding affinity Δ*G*: -7.86 kcal/mol). The docking picture obtained from the UCSF chimera software[31] is shown in Fig. 5. The docking result suggests that the title compounds have strong binding affinity toward target protein achieving the best FF score against 5KLH. Thus, the compounds might be used as active agent for transmission blocking therapy against TbPSSA-2.

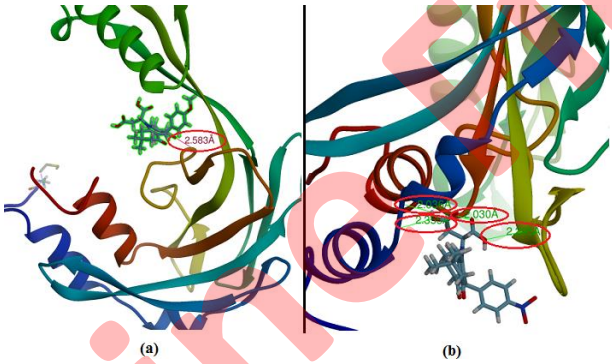

Fig. 5. Hydrogen bond interaction of (a) MTDOSA and (b) NTDOSA with 5KLH

CONCLUSIONS

The experimental (FT-IR, NMR and UV-Vis. techniques) and theoretical quantum chemical method have been employed to analyze the spectroscopic properties of MTDOSA and NTDOSA for the first time. The optimized geometric parameters and vibrational harmonic wave numbers, of the compounds have been calculated using DFT/B3LYP methods with 6-311++G (d,p) basis set. A good agreement between experimental and calculated normal modes of vibrations has been found and vibrational modes are successfully assigned using potential energy distribution. The calculated UV-Vis. absorption peaks in methanol of both the compounds match well with the experimentally observed absorption peaks. The calculated global reactivity parameters reveal that the compound NTDOSA is a good nucleophile while the compound MTDOSA is a good electrophile. The molecular docking results show that the compounds MTDOSA and NTDOSA have strong binding affinity toward target protein 5KLH. Thus, the compounds may be used as an antileishmanial drug.

SUPPLIMENTRY MATERIAL

The recorded ^{13}C and ^{1}H NMR spectra of NTDOSA and MTDOSA in DMSO solution is shown in Fig. S1 to Fig. S8. The HOMO-LUMO plots and MESP for both the molecules are shown in Figs. S9 and S10 respectively. The optimized geometric parameters for compounds MTDOSA and NTDOSA are listed in Tables SI and SII respectively. The vibrational analyses of prominent modes of the title compounds along with experimental data are given in Tables SIII and SIV. The Experimental and calculated absorption wavelengths, excitation energies, absorbance values and oscillator strengths of the MTDOSA and NTDOSA molecules are given in Tables SV and SVI respectively. The calculated and experimentally observed values of ^{1}H and ^{13}C chemical shifts of MTDOSA and NTDOSA for the proton and carbon atoms in DMSO solvent, taking tetramethylsilane (TMS) as a reference, are depicted in Tables SV and SVI, respectively. Characterization data of the synthesized compounds 4a and 4b are given in supplementary information.

ИЗВОД

СПЕКТРОСКОПСКО (FTIR, UV-Vis И NMR), ТЕОРИЈСКО ИСТРАЖИВАЊЕ И МОЛЕКУЛСКИ ДОКИНГ СУПСТИТУИСАНИХ ДЕРИВАТА 1,8-ДИОКСОДЕКАХИДРОАКРИДИНА

KRISHNA KANT YADAV[1], ABHISHEK KUMAR[1], SANCHARI BEGAM[2], KHONDEKAR NURJAMAL[2], AMARENDRA KUMAR[1], GOUTAM BRAHMACHARI[2] и NEERAJ MISRA1

[1]Department of Physics, University of Lucknow, Lucknow-226007, India;
[2]Laboratory of Natural Products & Organic Synthesis, Department of Chemistry, Visva-Bharati (a Central University), Santiniketan-731 235, West Bengal, India

Супституисани деривати 1,8-диоксодекахидроакридина недавно су истраживани и нађено је имају разноврсне биолошке и фармаколошке активности. Два од ових биолошки релевантних *N*-хетероцикличних скелета 2-(9-(4-метоксифенил)-3,3,6,6-тетраметил-1,8-диоксо-1,2,3,4,5,6,7,8-октахидро-акридин-10(9*H*)-ил)ћилибарна киселина (MTDOSA) и 2-(3,3,6,6-тетраметил-9-(4-нитрофенил)-1,8-диоксо-1,2,3,4,5,6,7,8-октахидроакридин-10(9*H*)-ил)ћилибарна киселина (NTDOSA) проучавани су у основном и првом ексцитованом стању користећи DFT метод на B3LYP/6-311++G(d,p) нивоу теорије. Квантно хемијска израчунавања геометрије структура и вибрационих таласних бројева за MTDOSA и NTDOSA изведена су користећи DFT метод. Експериментални FT-IR спектри једињења су снимљени у области 4000-400 cm^{-1} и свеобухватно су тумачени на основу расподеле потенцијалне енергије. Глобални дескриптори реактивности су израчунати и дискутовани. Надаље, израчунати су ^{1}H и ^{13}C NMR спектри користећи GIAO метод и упоређени су са експерименталним спектрима. Студија доковања показује да једињења MTDOSA и NTDOSA имају јак афинитет везивања за циљни протеин 5KLH. Тако, једињења могу имати примену као лек за лајмску болест.

(Примљено 28. децембра 2018; ревидирано 6. септембра 2019; прихваћено 16. септембра 2019)

REFERENCES

1. C. Santelli-Rouvier, B. Pradines, M. Berthelot, D. Parzy, J. Barbe, Eur. *J. Med. Chem.***39** (2004) 735 (https://dx.doi.org/10.1016/j.ejmech.2004.05.007)
2. T. L. Su, Y.W. Lin, T.C. Chou, X. Zhang, V. A. Bacherikov, C.H. Chen, L. F. Liu, T.J. Tsai, *J. Med. Chem.***49** (2006) 3710 (https://dx.doi.org/10.1021/jm060197r)

3. S. A. Gamage, D. P. Figgitt, S. J. Wojcik, R. K. Ralph, A. Ransijn, J. Mauel, V. Yardley, D. Snowdon, S. L. Croft, W. A. Denny, *J. Med. Chem.* **40** (1997) 2634 (https://dx.doi.org/10.1021/jm970232h)
4. R. A. Janis, D. J. Triggle, *J. Med. Chem.* **26** (1983) 775 (https://dx.doi.org/10.1021/jm00360a001)
5. M. Kaya, Y. Yıldırır, L. Terker, *J. Heterocyclic Chem.* **46** (2009) 294 (https://dx.doi.org/10.1002/jhet.45)
6. X.-S. Wang, M.-M. Zhang, Z.-S. Zeng, D.-Q. Shi, S.-J. Tu, X.-Y. Wei, Z.-M. Zong, *Tetrahedron Lett*. **46** (2005)7169 (https://dx.doi.org/10.1016/j.tetlet.2005.08.091)
7. B. Banerjee, G. Brahmachari, *J. Chem. Res.* **38** (2014)745 (https://dx.doi.org/10.3184/174751914X14177132210020)
8. G. Brahmachari, S. Begam, K. Nurjamal, *ChemistrySelect*, **2** (2017) 331 (https://dx.doi.org/10.1002/slct.201700265)
9. Gaussian 09, Revision A.1, M. J. Frisch, G. W. Trucks, H. B. Schlegel, G. E. Scuseria, M. A. Robb, J. R. Cheeseman, G. Scalmani, V. Barone, B. Mennucci, G. A. Petersson, H. Nakatsuji, M. Caricato, X. Li, H.P. Hratchian, A. F. Izmaylov, J. Bloino, G. Zheng, J. L. Sonnenberg, M. Hada, M. Ehara, K. Toyota, R. Fukuda, J. Hasegawa, M. Ishida, T. Nakajima, Y. Honda, O. Kitao, H. Nakai, T. Vreven, J.A. Montgomery, Jr., J. E. Peralta, F. Ogliaro, M. Bearpark, J. J. Heyd, E. Brothers, K. N. Kudin, V. N. Staroverov, R. Kobayashi, J. Normand, K. Raghavachari, A. Rendell, J. C. Burant, S. S. Iyengar, J. Tomasi, M. Cossi, N. Rega, J. M. Millam, M. Klene, J. E. Knox, J. B. Cross, V. Bakken, C. Adamo, J. Jaramillo, R. Gomperts, R. E. Stratmann, O. Yazyev, A. J. Austin, R. Cammi, C. Pomelli, J. W. Ochterski, R. L. Martin, K. Morokuma, V. G. Zakrzewski, G. A. Voth, P. Salvador, J. J. Dannenberg, S. Dapprich, A. D. Daniels, O. Farkas, J. B. Foresman, J. V. Ortiz, J. Cioslowski, D. J. Fox, *Gaussian, Inc.*, Wallingford CT, 2009
10. A. P. Scott, L. Radom, *J. Phys. Chem.***100** (1996) 16502 (https://dx.doi.org/10.1021/jp960976r)
11. P. Pulay, G. Fogarasi, G. Pongor, J. E. Boggs, A. Vargha, *J. Am. Chem. Soc.* **105** (1983) 7037 (https://dx.doi.org/10.1021/ja00362a005)
12. M. H. Jamroz, *Spectrochim. Acta A* **114** (2013) 220 (https://doi.org/10.1016/j.saa.2013.05.096)
13. M. Ladd, *Introduction to Physical Chemistry*, Third ed., Cambridge University Press, Cambridge, U.K. 1998 ISBN 0521480000
14. F. H. Allen, O. Kennard, D. G. Watson, L. Brammer, A. G. Orpen, R. Taylor, *J. Chem. Soc. Perkin Trans. II* **12** (1987) S1 (https://dx.doi.org/10.1039/P298700000S1)
15. D. Michalska, D. C. Bienko, A.J.Abkowicz-Bienko, Z. Latajaka, *J. Phys. Chem.* **100** (1996) 17786 (https://dx.doi.org/10.1021/jp961376v)
16. R. L. Pecsok, L. D. Shield, I. C. McWillam, *Modern Methods of Chemical Analysis*, Wiley, New York, U.S.A. 1976 ISBN 10: 0471676624/ISBM 13: 9780471676621.
17. P. K. Chattaraj, U. Sarkar, D.R. Roy, *Chem. Rev.* **106** (2006) 2065 (https://dx.doi.org/10.1021/cr040109f)
18. P. A. Johnson, L. J. P. Bartolotti, W. Ayers, T. Fievez, P. Geerlings, *Charge Density and Chemical Reactions: A Unified View from Conceptual DFT*, in *Modern Charge Density Analysis*,C.Gatti, P. Macchi (Eds.), Springer, New York, 2012 (https://dx.doi.org/10.1007/978-90-481-3836-4_21)
19. R. G. Parr, R. A. Donnelly, M. Levy, W. E. Palke, *J. Chem. Phys.* **68** (1978) 3801 (https://dx.doi.org/10.1063/1.436185)

20. R. G. P earson, *Inorg. Chim. Acta* **240** (1995) 93 (https://dx.doi.org/10.1016/0020-1693(95)04648-8)
21. P. W. Ayers, R. G. Parr, R. G. Pearson, *J. Chem. Phys.* **124** (2006) 194107 (https://dx.doi.org/10.1063/1.2196882)
22. P. W. Ayers, *Faraday Discuss.* **135** (2007) 161 **(**https://dx.doi.org/10.1039/B606877D)
23. R. G. Parr, L. Szentpaly, S. Liu, *J. Am. Chem. Soc*. **121** (1999) 1922 (https://dx.doi.org/10.1021/ja983494x)
24. S. B. Liu, *Electrophilicity*, in *Chemical Reactivity Theory: A Density Functional View*, P. K. Chattaraj, Ed., chapter 13, Taylor & Francis, Boca Raton, Fla, USA, 2009,p. 179
25. R. Parthasarathi, J. Padmanabhan , V. Subramanian, B. Maiti, P. K. Chattaraj, *Current Science* **86** (2004) 535 (https://www.currentscience.ac.in/Downloads/article_id_086_04_0535_0542_0.pdf)
26. J. A. War, K. Jalaja, Y. S. Mary, C. Y. Panicker, S. Armakovic, S. J. Armakovic, S. K. Srivastava, C. Van Alsenoy, *J. Mol. Struct.* **1129** (2017) 72 (https://dx.doi.org/10.1016/j.molstruc.2016.09.063)
27. I. Fleming, *Frontier Orbitals and Organic Chemical Reactions*, John Wiley and Sons, New York, USA 1976ISBN 978-0-470-74660-8 (H/B), 978-0-470-74659-2 (P/B)
28. E. Scrocco, J. Tomasi, *Electronic Molecular Structure, Reactivity and Intermolecular Forces: An Euristic Interpretation by Means of Electrostatic Molecular Potentials* in P. Lowdin (Ed.), *Advances in Quantum Chemistry*, Academic Press, New York, U.S.A. 1978 (https://dx.doi.org/10.1016/S0065-3276(08)60236-1)
29. A. Grosdidier, V. Zoete, O. Michielin, *Nucleic Acids Res.* **39** (2011) 270 (https://dx.doi.org/10.1093/nar/gkr366)
30. R. Ramaswamy, S. Goomeshi Nobary, B. A. Eyford, T. W. Pearson, M. J. Boulanger, *Protein Sci.* **25** (2016) 2297 (http://www.rcsb.org/pdb/explore/explore.do?structureId=5KLH)
31. E. F. Pettersen, T. D. Goddard, C. C. Huang, G. S. Couch, D. M. Greenblatt, E. C. Meng, T. E. Ferrin, *J. Comput. Chem.* **25** (2004) 1605 (https://dx.doi.org/10.1002/jcc.20084)

SUPPLEMENTARY MATERIAL TO

Spectroscopic (FTIR, UV-Vis and NMR), theoretical investigation and molecular docking of substituted 1,8-dioxodecahydroacridine derivatives

KRISHNA KANT YADAV[1], ABHISHEK KUMAR[1], SANCHARI BEGAM[2], KHONDEKAR NURJAMAL[2], AMARENDRA KUMAR[1], GOUTAM BRAHMACHARI[2] and NEERAJ MISRA[1]

[1]Department of Physics, University of Lucknow, Lucknow-226007, India; [2]Laboratory of Natural Products & Organic Synthesis, Department of Chemistry, Visva-Bharati (a Central University), Santiniketan-731 235, West Bengal, India

Characterization data of the synthesized compounds 4a and 4b:

2-(9-(4-Methoxyphenyl)-3,3,6,6-tetramethyl-1,8-dioxo-2,3,4,5,6,7,8,9-octahydroacridin-10(1*H*)-yl)succinic acid (**4a**). White solid: yield 86%; mp 255 °C; R_f (50% ethyl acetate/petrol ether) 0.69; IR (KBr): ν_{max} = 3312 (COOH), 3069, 3002, 2959, 2877, 2834, 2359, 1710(-COOH), 1668 (CO), 1606, 1510, 1461, 1360, 1301, 1260, 1233, 1194, 1163, 1137, 1108, 1031, 998, 934, 845, 776, 685, 637, 567, 532, 422 cm^{-1}; ^{1}H NMR (400 MHz, $CDCl_3$): δ = 7.17 (2H, d, *J* = 8.8 Hz, Ar-H), 6.73 (2H, d, *J* = 8.4 Hz, Ar-H), 4.78 (2H, s, -C*H* and NC*H*(COOH)), 4.67 (2H, br s, -CH_2-), 3.71 (3H, s, Ar-OCH_3), 2.44 (4H, s, 2 × -CH_2-), 2.23-2.19 (2H, m, -CH_2-), 2.16-2.12 (2H, m, -CH_2-), 1.08 (6H, s, 2 × -CH_3), 0.97 (6H, br s, 2 × -CH_3) ppm; ^{13}C NMR (100 MHz, $CDCl_3$): δ = 196.62 (2 × *C*O), 162.21 (2 × *C*OOH), 158.06 (2C), 136.59 (2C), 129.40 (3C), 115.88 (2C), 113.57 (2C), 93.52 (N-*C*), 55.21 (Ar-O*C*H_3), 50.86 (-*C*H_2-), 40.96 (2 × -COCH_2-), 32.27 (2 × -*C*H_2-), 31.05 (2C), 29.34 (2 × -*C*H_3), 27.43 (2 × -*C*H_3) ppm. Elemental analysis: calcd (%) for $C_{28}H_{33}NO_7$: C, 67.86; H, 6.71; N, 2.83; found: C, 67.94; H, 6.70; N, 2.80.

2-(3,3,6,6-tetramethyl-9-(4-nitrophenyl)-1,8-dioxo-2,3,4,5,6,7,8,9-octahydroacridin-10(1*H*)-yl)succinic acid (**4b**). White solid: yield 74%; mp 215 °C, R_f (50% ethyl acetate/petrol ether) 0.65; IR (KBr): ν_{max} = 3382 (COOH), 3117, 2956, 2866, 2360, 1731 (COOH), 1722 (COOH), 1665 (CO), 1593, 1474, 1386, 1299, 1194, 1114, 1017, 910, 858, 788, 750, 678, 660, 573, 523,461 cm^{-1}; ^{1}H NMR (400 MHz, DMSO-d_6): δ = 7.07 (2H, d, *J* = 8.4 Hz, Ar-H), 6.76 (2H, d, *J* = 8.8 Hz, Ar-H), 4.51 (1H, s, -C*H*), 2.69-2.59 (8H, m, 4 × -CH_2-), 2.34-2.33 (1H, m, -C*H*), 2.33-2.28 (2H, m, -CH_2-), 2.25 (3H, s, -CH_3), 1.94 (3H, s, -CH_3),

1.83 (3H, s, -CH_3), 1.23 (3H, s, -CH_3) ppm; ^{13}CNMR (100 MHz, DMSO-d_6): δ = 179.83 (*C*O), 177.45 (*C*O), 173.11 (-*C*OOH), 169.99 (-*C*OOH), 163.94, 146.14, 139.25, 129.49, 129.15, 127.47, 126.43, 114.87, 113.54, 107.62, 67.45 (N-*C*), 36.95 (-*C*H), 35.09 (2 × -CO*C*H_2-), 30.94 (-*C*H_2(COOH)), 26.84 (2 × -CH_2-), 24.55 (2C), 21.50 (2 × -*C*H_3), 15.83 (2 × -*C*H_3) ppm. Elemental analysis: calcd (%) for $C_{27}H_{30}N_2O_8$: C, 63.52; H, 5.92; N, 5.49; found: C, 63.58; H, 5.90; N, 5.51.

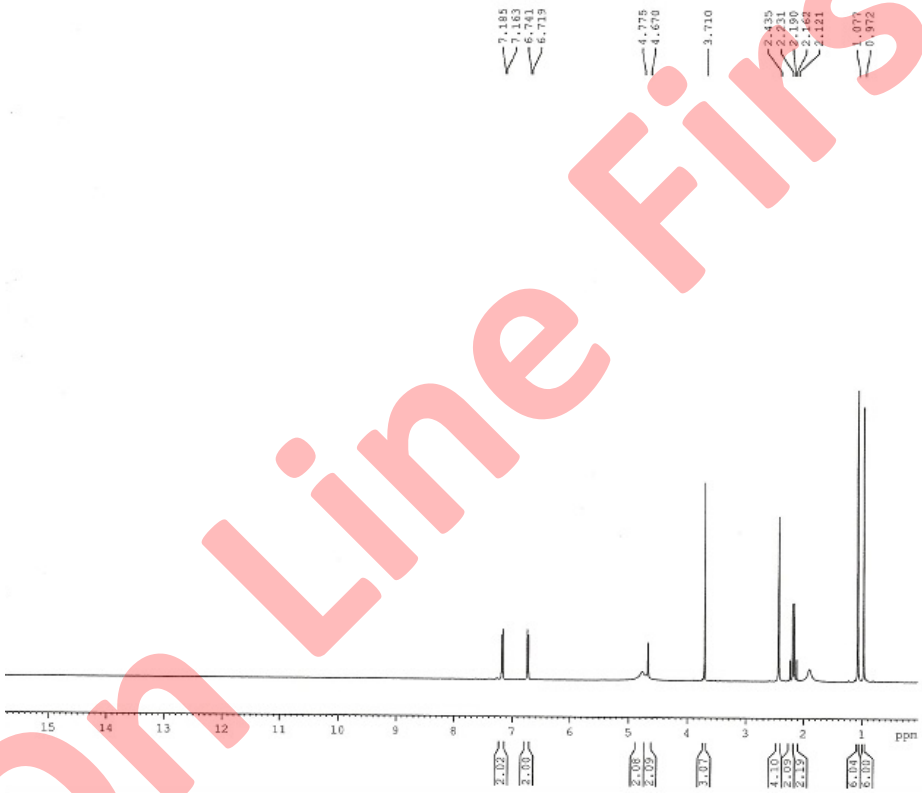

Fig. S1. Experimental ^{1}H NMR plot of MTDOSA

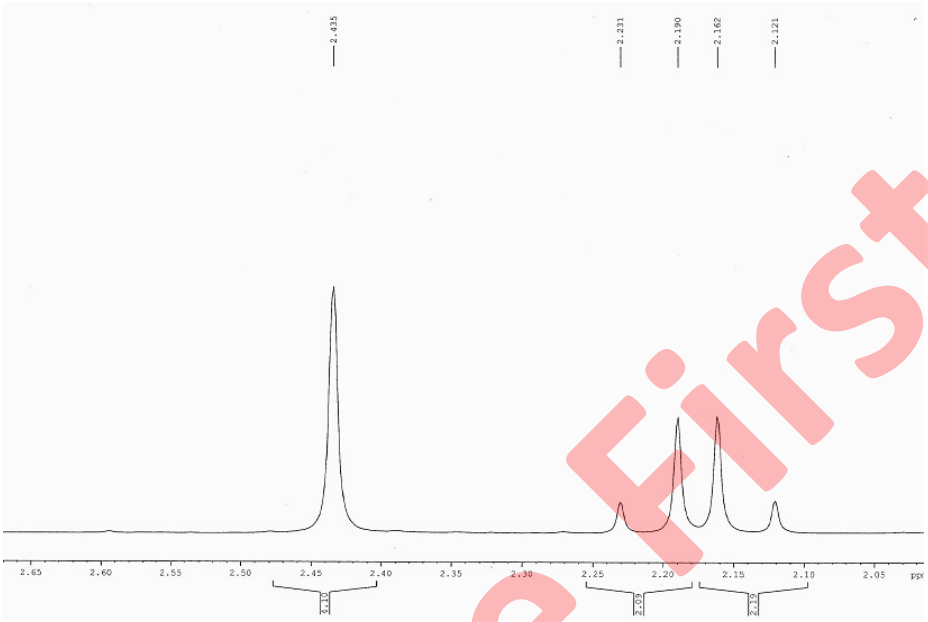

Fig. S2 Experimental ^{1}H NMR plot of MTDOSA (extended scale-I)

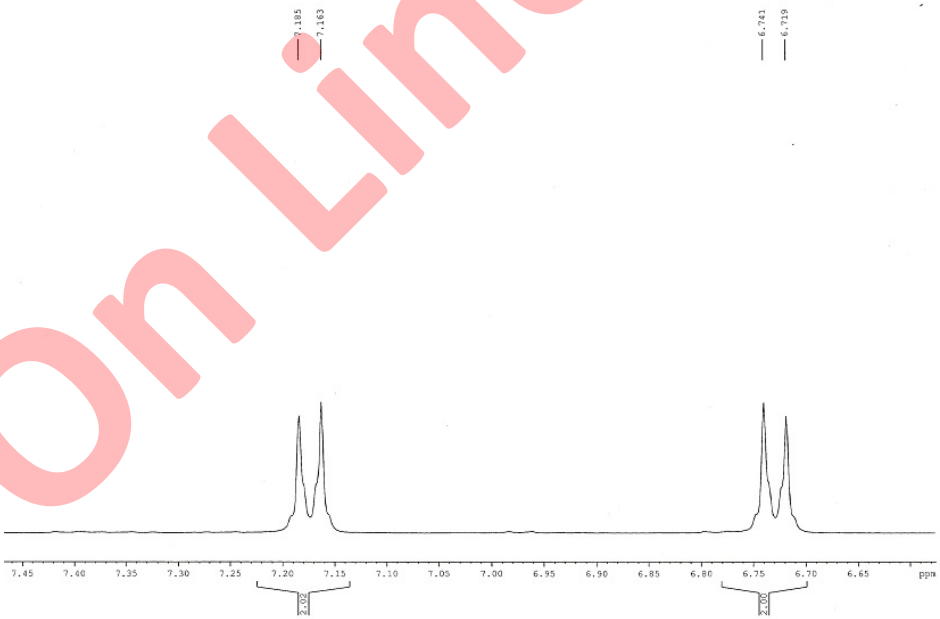

Fig. S3 Experimental ^{1}H NMR plot of MTDOSA (extended scale-II)

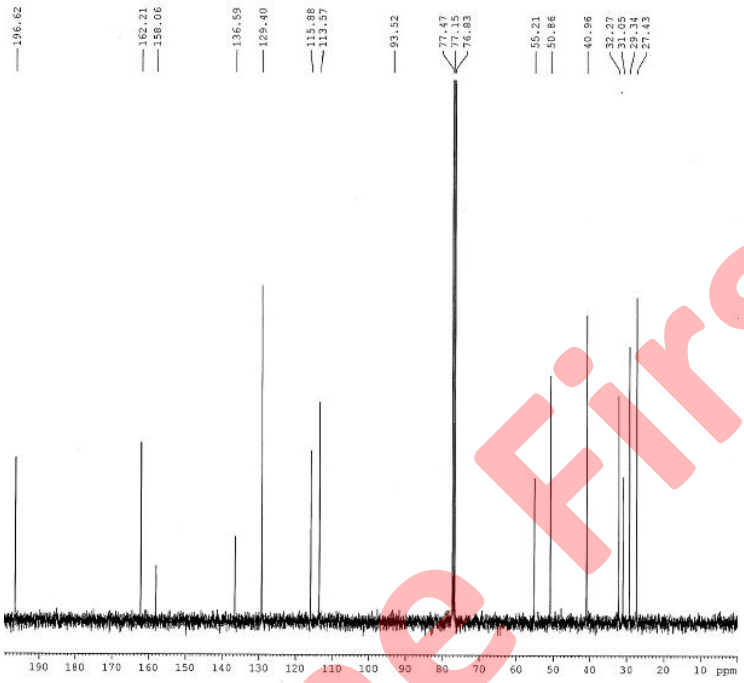

Fig. S4. Experimental ^{13}C NMR Plot of MTDOSA

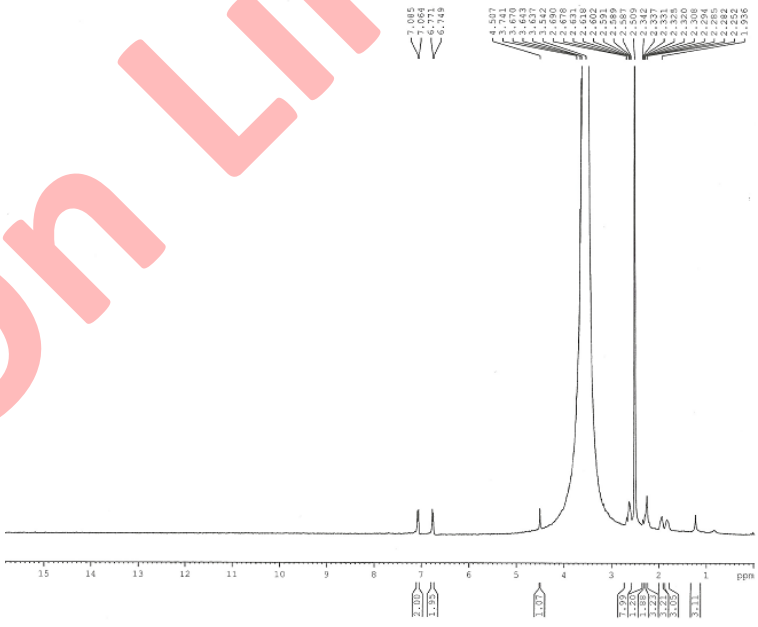

Fig. S5 Experimental ^{1}H NMR plot of NTDOSA

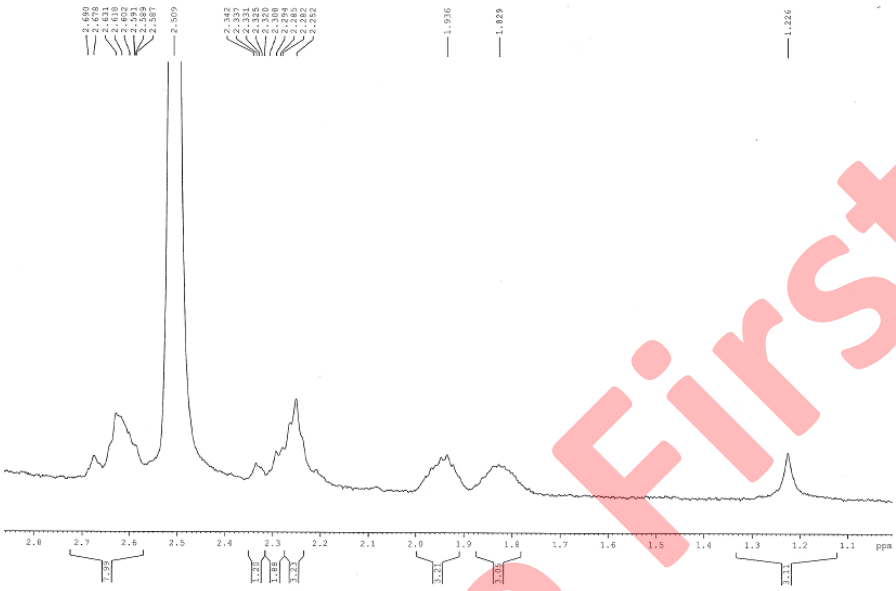

Fig. S6. Experimental ^{1}H NMR plot of NTDOSA (extended scale-I)

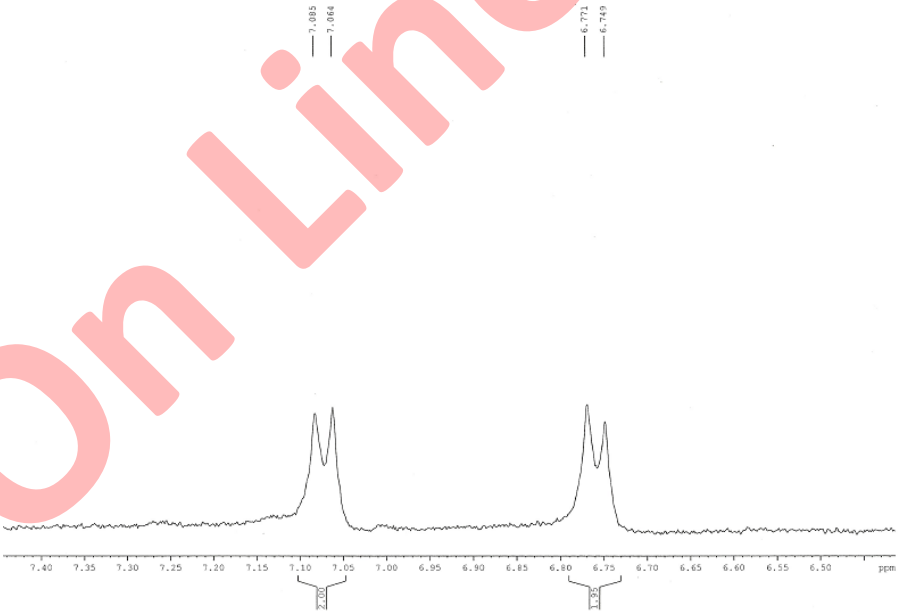

Fig. S7 Experimental ^{1}H NMR plot of NTDOSA (extended scale-II)

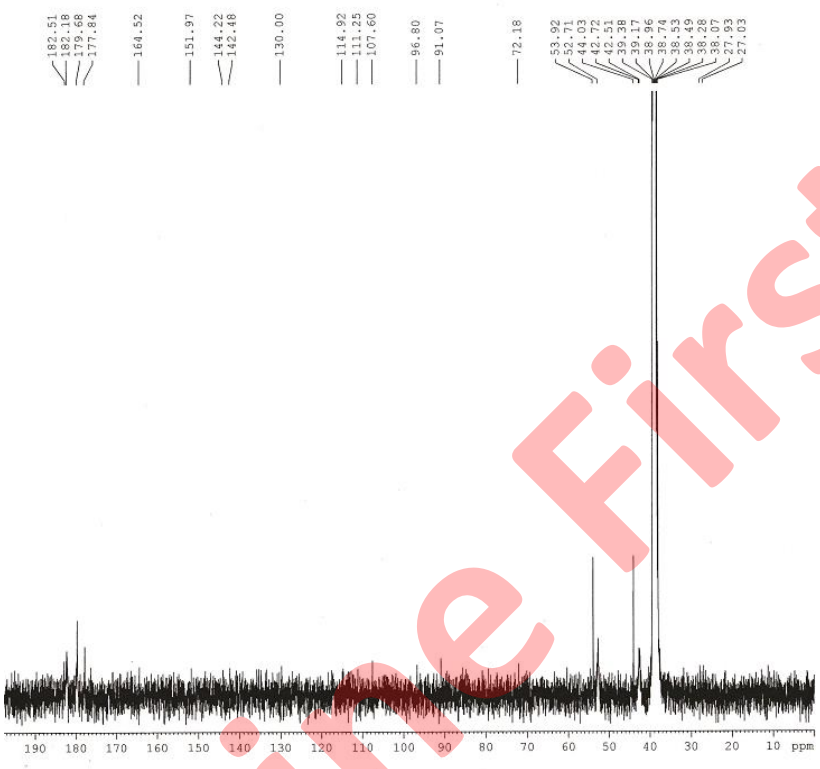

Fig. S8. Experimental ^{13}C NMR Plot of NTDOSA

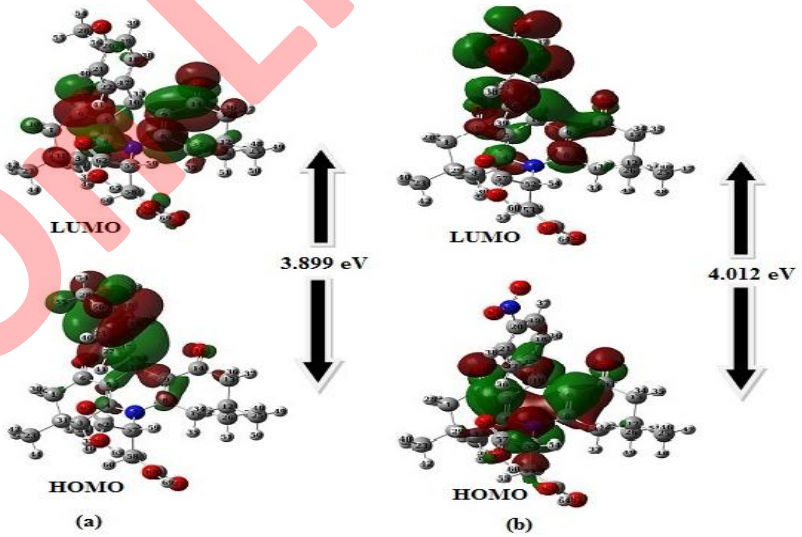

Fig. S9. HOMO, LUMO plots of (a) MTDOSA (b) NTDOSA molecules

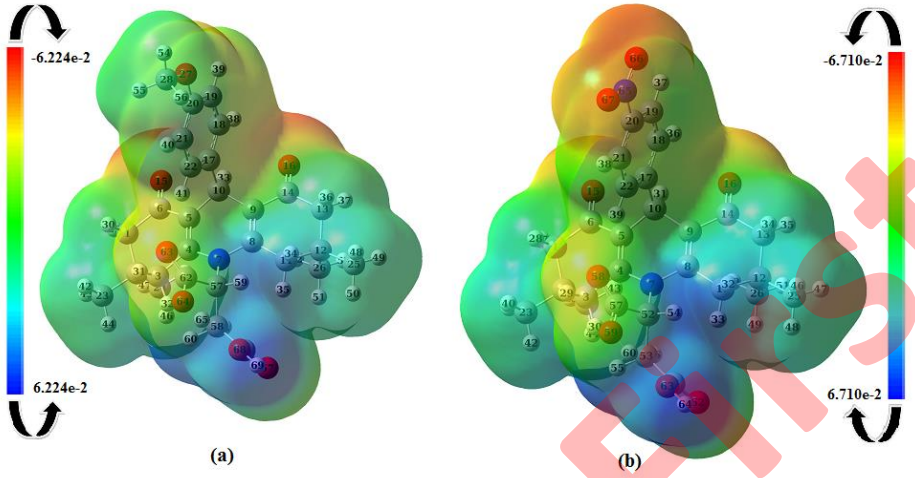

Fig. S10. MESP Surface for (a) MTDOSA (b) NTDOSA calculated at B3LYP/6- 311++G (d,p)

Table SI. Optimized geometric parameter for MTDOSA.

Parameter	DFT/B3LYP6311++G(d,p) Bond length, Å	Parameter	DFT/B3LYP6311++G(d,p) Dihedral angle, °
C1-C2	1.537	C6-C1-C2-C3	53.25
C1-C6	1.518	C6-C1-C2-C23	171.72
C2-C3	1.546	C6-C1-C2-C24	-67.97
C3-C4	1.515	C2-C1-C6-C5	-33.75
C4-C5	1.355	C2-C1-C6-O15	147.79
C4-N7	1.416	C1-C2-C3-C4	-59.60
C5-C6	1.476	C23-C2-C3-C4	-168.84
C5-C10	1.511	C24-C2-C3-C4	71.36
C6-O15	1.220	C2-C3-C4-C5	26.53
N7-C8	1.415	C2-C3-C4-N7	-151.00
N7-C57	1.461	C3-C4-C5-C6	-3.83
C8-C9	1.354	C3-C4-C5-C10	176.63
C8-C11	1.516	N7-C4-C5-C6	173.66
C9-C10	1.515	N7-C4-C5-C10	-5.87
C9-C14	1.475	C3-C4-CN7-C8	159.64
C10-C17	1.534	C3-C4-N7-C57	-23.90
C11-C12	1.547	C5-C4-N7-C8	-17.94
C12-C13	1.536	C3-C4-N7-C57	158.50
C12-C25	1.537	C4-C5-C6-C1	7.42
C12-C26	1.541	C4-C5-C6-O15	-174.13
C13-C14	1.519	C10-C5-C6-C1	-173.01
C14-O16	1.221	C10-C5-C6-O15	4.43
C17-C18	1.402	C4-C5-C10-C9	26.43
C17-C22	1.393	C4-C5-C10-C17	-99.03
C18-C19	1.386	C6-C5-C10-C9	-153.12

Parameter	DFT/B3LYP6311++G(d,p)	Parameter	DFT/B3LYP6311++G(d,p)
	Bond length, Å		Dihedral angle, º
C19-C20	1.399	C6-C5-C10-C17	81.41
C20-C21	1.395	C4-N7-C8-C9	17.88
C20-O27	1.369	C4-N7-C8-C11	-159.18
C21-C22	1.398	C57-N7-C8-C9	-158.71
O27-C28	1.418	C57-N7-C8-C11	24.21
C57-C58	1.576	C4-N7-C57-C58	79.23
C57-C62	1.551	C4-N7-C57-C62	-52.58
C58-C66	1.511	C8-N7-C57-C58	-104.31
C62-O63	1.197	C8-N7-C57-C62	123.87
C62-O64	1.346	N7-C8-C9-C10	6.00
O64-H65	0.973	N7-C8-C9-C14	-173.13
C66-O67	1.198	C11-C8-C9-C10	-177.07
C66-O68	1.372	C11-C8-C9-C14	3.79
O68-H69	0.97	N7-C8-C11-C12	151.92
	Bond Angle, º	C9-C8-C11-C12	-25.08
C2-C1-C6	113.48	C8-C9-C10-C5	-26.41
C1-C2-C3	107.84	C8-C9-C10-C17	99.90
C1-C2-C23	109.97	C14-C9-C10-C5	152.75
C1-C2-C24	110.42	C14-C9-C10-C17	-80.94
C3-C2-C23	108.77	C8-C9-C14-C13	-8.69
C3-C2-C24	110.83	C8-C9-C14-O16	172.84
C23-C2-C24	108.98	C10-C9-C14-C13	172.14
C2-C3-C4	114.11	C10-C9-C14-O16	-6.32
C3-C4-C5	121.87	C5-C10-C17-C18	-149.36
C3-C4-N7	118.33	C5-C10-C17-C22	41.44
C5-C4-N7	119.74	C9-C10-C17-C18	96.70
C4-C5-C6	120.89	C9-C10-C17-C22	-82.49
C4-C5-C10	122.20	C8-C11-C12-C13	48.17
C6-C5-C10	116.90	C8-C11-C12-C25	167.80
C1-C6-C5	117.96	C8-C11-C12-C26	-72.65
C1-C6-O15	120.76	C11-C12-C13-C14	-53.15
C5-C6-O15	121.27	C25-C12-C13-C14	-172.02
C4-N7-C8	118.69	C26-C12-C13-C14	67.63
C4-N7-C57	122.68	C12-C13-C14-C9	34.93
C8-N7-C57	118.52	C12-C13-C14-O16	-146.59
N7-C8-C9	120.31	C10-C17-C18-C19	-179.00
N7-C8-C11	117.41	C22-C17-C18-C19	-0.21
C9-C8-C11	122.22	C10-C17-C22-C21	179.05
C8-C9-C10	121.61	C18-C17-C22-C21	-0.15
C8-C9-C14	120.79	C17-C18-C19-C20	-0.14
C10-C9-C14	117.58	C18-C19-C20-C21	0.01
C5-C10-C9	109.09	C18-C19-C20-O27	-179.77
C5-C10-C17	113.38	C19-C20-C21-C22	0.07
C9-C10-C17	111.93	O27-C20-C21-C22	179.81

Parameter	DFT/B3LYP6311++G(d,p) Bond Angle, º	Parameter	DFT/B3LYP6311++G(d,p) Dihedral angle, º
C8-C11-C12	114.22	C19-C20-O27-C28	178.73
C11-C12-C13	108.10	C21-C20-O27-C28	-1.02
C11-C12-C25	108.90	C20-C21-C22-C17	0.02
C11-C12-C26	110.34	N7-C57-C58-C66	129.19
C13-C12-C25	110.11	C62-C57-C58-C66	-99.43
C13-C12-C26	110.41	N7-C57-C62-O63	-1.65
C25-C12-C26	108.96	N7-C57-C62-O64	-179.67
C12-C13-C14	113.47	C58-C57-C62-O63	-133.63
C9-C14-C13	117.88	C58-C57-C62-O64	48.34
C9-C14-O16	121.44	C57-C58-C66-O67	-124.96
C13-C14-O16	120.66	C57-C58-C66-O68	55.32
C10-C17-C18	119.85	C21-C20-O27-C28	-1.02
C10-C17-C22	122.16	C20-C21-C22-C17	0.02
C18-C17-C22	117.98	N7-C57-C58-C66	129.19
C17-C18-C19	121.23	C62-C57-C58-C66	-99.43
C18-C19-C20	120.17	N7-C57-C62-O63	-1.65
C19-C20-C21	119.46	N7-C57-C62-O64	-179.67
C19-C20-O27	115.94	C58-C57-C62-O63	-133.63
C21-C20-O27	124.61	C58-C57-C62-O64	48.34
C20-C21-C22	119.67	C57-C58-C66-O67	-124.96
C17-C22-C21	121.49		
C20-O27-C28	118.42		
N7-C57-C58	114.08		
C58-C57-C62	113.74		
C57-C58-C66	114.52		
C57-C62-O63	124.04		
C57-C62-O64	115.14		
O63-C62-O64	120.79		
C58-C66-O67	126.75		
C58-C66-O68	111.28		
O67-C66-O68	121.96		

Table SII. Optimized geometric parameters for NTDOSA.

Parameter	DFT/B3LYP6311++G(d,p) Bond length, Å	Parameter	DFT/B3LYP6311++G(d,p) Dihedral angle, º
C1-C2	1.538	C6-C1-C2-C3	52.83
C1-C6	1.517	C6-C1-C2-C23	171.23
C2-C3	1.548	C6-C1-C2-C24	-68.48
C2-C23	1.538	C2-C1-C6-C5	-32.48
C2-C24	1.541	C2-C1-C6-O15	159.65
C3-C4	1.514	C1-C2-C3-C4	-49.73
C4-C5	1.355	C23-C2-C3-C4	-169.93
C4-N7	1.415	C24-C2-C3-C4	71.35
C5-C6	1.476	C2-C3-C4-C5	26.26
C5-C10	1.510	C2-C3-C4-N7	-151.12
C6-O15	1.221	C3-C4-C5-C6	-2.74
N7-C8	1.4132	C3-C4-C5-C10	177.47
N7-C52	1.4637	N7-C4-C5-C6	174.61
C8-C9	1.355	N7-C4-C5-C10	-5.16
C8-C11	1.516	C3-C4-N7-C8	159.78
C9-C10	1.515	C3-C4-N7-C52	-24.86
C9-C14	1.475	C5-C4-N7-C8	-17.68
C10-C17	1.534	C5-C4-N7-C52	157.69
C11-C12	1.547	C4-C5-C6-C1	5.82
C12-C13	1.573	C4-C5-C6-O15	-176.03
C12-C25	1.537	C10-C5-C6-C1	-174.38
C12-C26	1.542	C10-C5-C6-O15	3.75
C13-C14	1.517	C4-C5-C10-C9	24.95
C14-O16	1.221	C4-C5-C10-C17	-100.29
C17-C18	1.400	C6-C5-C10-C9	-154.83
C17-C22	1.400	C6-C5-C10-C17	79.91
C18-C19	1.389	C4-N7-C8-C9	17.54
C19-C20	1.391	C4-N7-C8-C11	-159.31
C20-C21	1.391	C52-N7-C8-C9	-157.99
C20-N65	1.475	C52-N7-C8-C11	25.14
C21-C22	1.390	C4-N7-C52-C53	79.63
C52-C53	1.574	C4-N7-C52-C57	-52.35
C52-C57	1.552	C8-N7-C52-C53	-105.01
C53-C61	1.511	C8-N7-C52-C57	123.01
C57-O58	1.198	N7-C8-C9-C10	5.38
C57-O59	1.344	N7-C8-C9-C14	-173.33
C61-O62	1.198	C11-C8-C9-C10	-177.89
C61-O63	1.371	C11-C8-C9-C14	3.38
N65-O66	1.226	N7-C8-C11-C12	151.56
N65-O67	1.227	C9-C8-C11-C12	-25.25

Parameter	DFT/B3LYP6311++G(d,p) Bond angle, º	Parameter	DFT/B3LYP6311++G(d,p) Dihedral angle, º
C2-C1-C6	113.55	C8-C9-C10-C5	-24.99
C1-C2-C3	107.96	C8-C9-C10-C17	101.23
C1-C2-C23	109.92	C14-C9-C10-C5	153.77
C1-C2-C24	110.48	C14-C9-C10-C17	-79.99
C3-C2-C23	108.67	C8-C9-C14-C13	-7.80
C3-C2-C24	110.45	C8-C9-C14-C16	173.90
C23-C2-C24	108.97	C10-C9-C14-C13	173.41
C2-C3-C4	113.11	C10-C9-C14-O16	-4.87
C3-C4-C5	121.67	C5-C10-C17-C18	-138.92
C3-C4-N7	118.40	C5-C10-C17-C22	41.97
C5-C4-N7	119.87	C9-C10-C17-C18	97.10
C4-C5-C6	121.13	C9-C10-C17-C22	-81.99
C4-C5-C10	122.31	C8-C11-C12-C13	48.43
C6-C5-C10	116.55	C8-C11-C12-C25	168.02
C1-C6-C5	118.04	C8-C11-C12-C26	-72.36
C1-C6-O15	121.98	C11-C12-C13-C14	-52.92
C5-C6-O15	120.94	C25-C12-C13-C14	-171.74
C4-N7-C8	118.74	C26-C12-C13-C14	67.84
C4-N7-C52	122.51	C12-C13-C14-C9	34.15
C8-N7-C52	118.58	C12-C13-C14-O16	-147.55
N7-C8-C9	120.46	C10-C17-C18-C19	-178.81
N7-C8-C11	117.42	C10-C17-C22-C21	178.78
C9-C8-C11	122.02	C18-C17-C22-C21	-0.32
C8-C9-C10	121.68	C17-C18-C19-C20	0.012
C8-C9-C14	120.94	C18-C19-C20-C21	-0.29
C10-C9-C14	117.35	C18-C19-C20-N65	179.90
C5-C10-C9	109.29	C19-C20-C21-C22	0.28
C5-C10-C17	113.35	N65-C20-C21-C22	-179.91
C9-C10-C17	111.66	C19-C20-N65-O66	0.01
C8-C11-C12	114.23	C19-C20-N65-O67	-179.85
C11-C12-C13	108.11	C21-C20-N65-O66	-179.80
C11-C12-C25	108.88	C21-C20-N65-O67	0.33
C11-C12-C26	110.34	C20-C21-C22-C17	-0.02
C13-C12-C25	110.08	N7-C52-C53-C61	130.24
C13-C12-C26	110.38	C57-C52-C53-C61	-98.68
C25-C12-C26	109.02	N7-C52-C57-O58	-3.19
C12-C13-C14	113.53	N7-C52-C57-O59	178.86
C9-C14-C13	117.95	C53-C52-C57-O58	-135.10
C9-C14-O16	121.18	C53-C52-C57-O59	46.95
C13-C14-O16	120.83	C52-C53-C61-O62	-122.93
C10-C17-C18	119.58	C52-C53-C61-O63	57.14
C10-C17-C22	121.48	N65-C20-C21-C22	-179.91
C18-C17-C22	118.92	C19-C20-N65-O66	0.01
C17-C18-C19	120.94	C19-C20-N65-O67	-179.85

Parameter	DFT/B3LYP6311++G(d,p)	Parameter	DFT/B3LYP6311++G(d,p)
	Bond angle, º		Dihedral angle, º
C18-C19-C20	118.77	C21-C20-N65-O66	-179.80
C19-C20-C21	121.68	C21-C20-N65-O67	0.33
C19-C20-N65	119.20	C20-C21-C22-C17	-0.02
C21-C20-N65	119.11	N7-C52-C53-C61	130.24
C20-C21-C22	118.81	C57-C52-C53-C61	-98.68
C17-C22-C21	120.86	N7-C52-C57-O58	-3.19
N7-C52-C53	114.06	N7-C52-C57-O59	178.86
N7-C52-C57	112.32	C53-C52-C57-O58	-135.10
C53-C52-C57	114.21	C53-C52-C57-O59	46.95
H54-C52-C57	102.47		
C52-C53-C61	114.29		
C52-C57-O58	125.45		
C52-C57-O59	115.45		
O58-C57-O59	120.92		
C57-O59-H60	113.01		
C53-C61-O62	126.68		
C53-C61-O63	111.22		
O62-C61-O63	122.09		
C61-O63-H64	109.16		
C20-N65-O66	117.88		
C20-N65-O67	117.85		
O66-C65-O67	124.27		

Table. SIII. Vibrational analysis of prominent modes of MTDOSA at the B3LYP/6-311++G(d,p) level.

Frequency, cm^{-1}			Assignment
Cal.	Scaled	Exp. FTIR	
3753	3630	3630	ν_{as}[O-H)(99)]
3644	3523	3312	ν_{s}[O-H)(99)]
3203	3097	3069	ν_{as}[C-H)R1(94)]
3195	3090		ν_{as}[C-H)R1(98)]
3188	3083		ν_{s}[C-H)R1(89)]
3180	3075		ν_{as}[C-H)R1(98)]
3148	3045		ν_{as}[C-H) CH_2 (98)]
3127	3024		ν_{as}[C-H) CH_3-O (91)]
3104	3002	3002	ν_{as}[C-H)R2 (91)]
3099	2997		ν_{as}[C-H)CH_3-R4 (76)]
3098	2996		ν_{as}[C-H)CH_3-R2(64)]
3097	2995		ν[C57-H59 (94)]
3090	2988		ν_{s}[C-H)CH_3-R4 (54)]
3089	2987		ν_{as}[C-H)CH_3-R2(83)]
3085	2983		ν_{as}[C-H)CH_3-R4(68)]
3083	2981		ν[C-H)R2 (54)]
3083	2981		ν_{as}[C-H){R2(44)+CH_3-R2(26)}]

Frequency, cm^{-1}			Assignment
Cal.	Scaled	Exp. FTIR	
3081	2979		ν_{as}[(C-H){R2+R3+CH_3-R2}(70)]
3080	2979		ν_{as}[(C-H){R2+R3+CH_3-R2}(70)]
3077	2976		ν_{as}[C-H)CH_3-R4(89)]
3075	2974		ν_{as}[C-H)CH_3-R2(84)]
3061	2960	2959	ν_{as}[C-H)R4 (69)]
3058	2957		ν_s[C-H)CH_2 (87)]
3055	2954		ν_{as}[C-H)CH_3-O-R1(100)]
3043	2943		ν_s[C-H)R2 (79)]
3026	2926		ν_s[C-H)CH_3-R4 (87)]
3023	2923		ν_s[C-H)CH_3-R2 (31)]
3016	2916		ν_s[C-H)CH_3-R4 (71)]
3015	2915		ν_{as}[C-H)CH_3-R2(78)]
3007	2908		ν_s[C-H)R2 (73)]
3004	2905		ν_s[C-H)R24(76)]
2999	2900		ν_s[C-H)CH_3-O-R1(91)]
2985	2886	2877	ν_s[C-H)R4 (72)]
1846	1785	1808	ν_s[(O=C)COOH(74)]
1836	1776	1731	ν_s[(O=C)COOH(82)]
1722	1665	1668	ν_s[(O=C)R2+R4(89)]
1716	1660		ν[(O=C)R4(64)]
1678	1622	1618	ν_s[(C=C)R3(68)]
1648	1593	1600	ν_{as}[C-C)R1(62)]+ β [(H-C-C)R1(19)]
1627	1573	1575	ν_{as} [(C=C)R3(71)]
1616	1563	1556	ν_{as}[C-C)R1(43)]
1540	1489	1510	β [(H-C-C)R1(48)]
1514	1464		β_O [(H-C-H)CH_3-R2(48)]
1513	1463	1461	β_O [(H-C-H)CH_3-R4(59)]
1507	1457		β_O [(H-C-H)CH_3-R4(55)]
1506	1456		β_O [(H-C-H)CH_3-R2(51)]
1505	1456		β_O [(H-C-H)CH_3-0-R1(72)]
1500	1450		β_O [(H-C-H)CH_3-R2+R2(39)]
1498	1449		β_O [(H-C-H)CH_3-R4+R4(52)]
1491	1442		β_O [(H-C-H)CH_3-O-R1(73)]
1490	1441		β_O [(H-C-H)CH_3-R2+R2(54)]
1489	1440	1440	β_O [(H-C-H)CH_3-R4(34)]
1483	1434	1434	β_O [(H-C-H)CH_3-R2+R2(56)]
1481	1433		β_O [(H-C-H)R4+CH_2(43)]
1475	1427		β_O [(H-C-H)R4+CH_2(64)]
1474	1426		β_O [(H-C-H)CH_3-O-R1(84)]
1463	1415		β_O [(H-C-H)CH_3-R4+R4(73)]
1461	1413		β_O [(H-C-H)CH_3-R2+R2(61)]
1455	1407		β [(H-C-C)R1(30)]
1439	1391		τ_i[{(H-C-C-N)(R3+R4)+(H-C-C-O)(COOH)}(22)]
1424	1377		β_O [(H-C-H)CH_3-R4(42)]

Frequency, cm^{-1}			Assignment
Cal.	Scaled	Exp. FTIR	
1423	1376		β_O [(H-C-H)CH_3-R1+R1(74)]
1403	1356	1360	β_O [(H-C-H)CH_3-R4(79)]
1402	1357		β_O [(H-C-H)CH_3-R1(22)]
1385	1339	1328	τ_i[{(H-C-C-N)(R3+R4)+(H-C-C-O)(COOH)}(18)]
1361	1316		β [(H-O-C)COOH(63)]
1352	1308		ν_s[C6-C5+C14-C9) (20)]
1346	1301	1301	β_O [(H-C-H)CH_2-R4(23)]
1340	1295		ν_s[(C-C)R1 (20)]+ β [(H-C-C)R1(57)]
1318	1275	1260	β [(H-O-C)COOH(19)]
1268	1226	1233	ν[O27-C20) (34)]
1264	1222		ν_{as}[(N-C)R3 (17)]
1249	1208		ν[N7-C57) (20)]
1235	1195	1194	β_O [(H-C-C)CH_2(34)]
1204	1164	1163	β [(H-C-C)R1(58)]
1201	1161		τ_i[(H-C-O-C)CH3-O-R1(48)]
1183	1143		ν[(O-C) COOH(17)]
1168	1130	1137	β_O [(H-C-H)CH_3-O-R1(19)]+ τ_i[(H-C-O-C)CH3-O-R1(54)]
1146	1108	1106	ν[(O-C) COOH(26)]+ β [(H-O-C)COOH(19)]
1142	1104		β_O [(H-C-C)R2(21)]
1139	1101		β_O [(H-C-C)R1(25)]
1136	1099		β [(H-C-C)R1(34)]
1123	1086		ν[(C-C) R1+R2(20)]
1063	1028	1031	ν[O27-C28) (72)]
1036	1002		τ_i[(H-C-C-C)CH3-R4+R4(21)]
1034	999	998	τ_i[(H-C-C-C)CH3-R2(21)]
1027	993		β [(H-C-C)R1(19)]+ β [(C-C-C)R1(60)]
985	953		τ_i[(H-C-C-C)R1(86)]
968	936	934	τ_i[(H-C-C-C)R1(51)]
948	917		τ_i[(H-C-C-C)CH_3-R1(20)]
944	913	910	β [(C-C-N)R1+R2+R3(20)]
905	875	882	τ_i[(H-C-C-C)R2(26)]
864	836	845	τ_i[(H-C-C-C)R1(24)]
826	799	806	τ_i[(H-C-C-C)R1(66)]
784	758	776	ν[O27-C20) (18)]
760	735	722	τ_o[(O-C-O-C)COOH(41)]
688	665	685	τ_i[(H-O-C-C)COOH(20)]
666	644	651	τ_i[(H-O-C-C)COOH(38)]
644	623	637	τ_o [{(O15-C1-C5-C6)(R2+(O-C-O-C)(COOH)}(18)]
642	621	606	β [(O-C-O)COOH(20)]
597	577	567	τ_i[(H-O-C-C)COOH(24)]
541	523	532	τ_i[(H-O-C-C)COOH(27)]
426	412	422	τ_i[(C-C-C-C)R1+R3(75)]
399	386	415	β [(C58-C57-N7)(19)]
392	379		β [(O-C-C)COOH(42)]

Frequency, cm^{-1}			Assignment
Cal.	Scaled	Exp. FTIR	
385	373		τ_o[(H-C-C-C)R2(23)]
285	275		β [(C-O-C)CH_3-O-R1(22)]
237	229		τ_i[(H-C-O-C)CH_3-O-R1(46)]
228	220		τ_i[(H-C-C-C)CH_3-R2(22)]
222	215		τ_i[(H-C-C-C)CH_3-R4+R4(19)]
152	147		τ_i[(H-C-C-C)CH_3-R4+R4(18)]
141	136		β [(C-C-C)R2+R4(20)]
106	102		τ_i[(C-C-C-C)R2(24)]
84	81		τ_i[(C-C-C-C)CH_3-O-R1(24)]
79	76		τ_i[(C-C-C-C)CH_3-O-R1(20)]
63	61		τ_i[(O-C-C-C)COOH(35)]
61	59		τ_i[(C-C-C-C)R1+R2+R3+R4(26)]
43	42		τ_i[(C57-C4-C8-N7)(27)]

ν: stretching; ν_s: symmetric stretching; ν_{as}: anti-symmetric stretching; β: bending in-plane; β_O: bending out-of-plane; τ_i: torsion in plane; τ_o: torsion out-of-plane

Table SIV. Vibrational analysis of prominent modes of NTDOSA at the B3LYP/6-311++G (d, p) level

Frequency, cm^{-1}			Assignment
Cal.	Scaled	Exp. FTIR	
3751	3627	3631	ν_{as}[(O-H)COOH(100)]
3637	3517	3312	ν_s[(O-H)COOH(99)]
3221	3115		ν_s[C-H)R1(91)]
3220	3114		ν_{as}[C-H)R1(92)]
3200	3094		ν_s[C-H)R1(82)]
3199	3093	3069	ν_{as}[C-H)R1(82)]
3148	3045		ν_{as}[C-H) CH_2 (90)]
3104	3002	3002	ν_{as}[C-H)R2(82)]
3099	2997		ν_{as}[C-H) CH_3-R4 (79)]
3096	2993		ν[C52-H54)(95)]
3091	2989		ν_{as}[C-H) CH_3-R4 (46)]
3090	2988		ν_{as}[C-H) CH_3-R2 (82)]
3087	2985		ν_{as}[C-H) CH_3-R4 (69)]
3086	2983		ν_{as}[C-H) CH_3-R2+R2 (77)]
3085	2983		ν_{as}[C-H) R4 (62)]
3082	2981		ν_{as}[C-H) CH_3-R2+R2 (26)]
3080	2979		ν[C-H)R3(90)]
3080	2978		ν_{as}[C-H) CH_3-R4 (87)]
3077	2975		ν_{as}[C-H) CH_3-R2 (83)]
3063	2962		ν[C-H)R4(71)]
3060	2959	2959	ν[C53-H56)(87)]
3041	2941		ν_{as}[C-H) R2 (78)]
3027	2927		ν_s[C-H) CH_3-R4 (79)]
3024	2924		ν_s[C-H) CH_3-R2 (29)]
3017	2918		ν_s[C-H) CH_3-R4 (70)]
3016	2916		ν_s[C-H) CH_3-R4 (70)]

Frequency, cm^{-1}			Assignment
Cal.	Scaled	Exp. FTIR	
3009	2909		ν_s[C-H) R2 (74)]
3006	2907		ν_s[C-H) R4 (74)]
2988	2889	2877	ν_s[C-H) R4 (73)]
1845	1784	1808	ν_s[O=C) COOH (84)]
1835	1775	1731	ν_s[O=C) COOH (82)]
1721	1665	1668	ν_s[O=C) R2+R4 (90)]
1716	1659		ν[O=C) R2 (68)]
1678	1623	1618	ν_s[C=C) R3 (67)]
1642	1588	1586	ν_{as}[C-C) R1(36)]
1633	1579	1576	ν_{as}[C-C) R1(28)]+ β [(H-C-C)R1(18)]
1624	1571	1556	ν_{as}[C=C) R3 (73)]
1569	1517	1510	ν_{as}[(O-N) NO_2 (77)]
1523	1472		β [(H-C-C)R1(63)]
1514	1464		β_O [(H-C-H)CH_3-R2(40)]
1513	1463	1461	β_O [(H-C-H)CH_3-R4(61)]
1508	1458		β_O [(H-C-H)CH_3-R4(57)]
1506	1457		β_O [(H-C-H)CH_3-R2(56)]
1499	1449		β_O [(H-C-H)CH_3-R4+R4(57)]
1498	1448		β_O [(H-C-H)CH_3-R2+R2(66)]
1490	1441	1440	β_O [(H-C-H)CH_3-R2+R2(51)]
1489	1440		β_O [(H-C-H)CH_3-R4(42)]
1482	1433	1434	β_O [(H-C-H)R4+CH_2(54)]
1481	1432		β_O [(H-C-H)CH_3-R2+R2(55)]
1477	1428		β_O [(H-C-H)R4+CH_2(66)]
1463	1414		β_O [(H-C-H)CH_3-R4+R4(71)]
1461	1413		β_O [(H-C-H)CH_3-R2+R2(61)]
1454	1406		ν_{as}[C-C) R1(19)]+ β [(H-C-C)R1(25)]
1436	1389		τ_i[{(H-C-C-N)(R3+R4)+(H-C-C-O)(COOH)}(21)]
1427	1380		β_O [(H-C-H)CH_3-R4(60)]
1423	1376		β_O [(H-C-H)CH_3-R2+R2(90)]
1405	1359	1360	β_O [(H-C-H)CH_3-R4(87)]
1402	1356		β_O [(H-C-H)CH_3-R2(42)]
1384	1338	1328	τ_i[{(H-C-C-N)(R3+R4)+(H-C-C-O)(COOH)}(16)]
1366	1321		ν_s[C-H) NO_2-R1 (66)]
1361	1316		β [(H-O-C)COOH(54)]
1355	1310		ν_s[C-C) R2+R4(16)]
1346	1302	1301	β [(H-C-C)R1(28)]+ β_O [(H-C-C)R2+CH_2(17)]
1343	1299		β [(H-C-C)R1(28)]
1319	1276		β [(H-O-C)COOH(16)]
1296	1253		β [(H-O-C)COOH(19)]
1265	1223		ν_{as}[(N-C) R3(19)]
1248	1207		ν_{as}[(N-C) R3(34)]
1233	1192		β_O [(H-C-C)COOH(34)]
1211	1171		β [(H-C-C)R1(51)]
1209	1169		β [(H-C-C)R1(16)]
1187	1148	1137	ν_{as}[O-C) COOH(19)]
1145	1107	1108	ν_{as}[O-C) COOH(24)]+ β [(H-O-C)COOH(17)]

Frequency, cm^{-1}			Assignment
Cal.	Scaled	Exp. FTIR	
1143	1105		β_O [(H-C-H)R2(23)]
1140	1102		β_O [(H-C-H)R4(23)]
1135	1097		β [(H-C-C)R1(46)]
1122	1085		ν_{as}[C-C) R2+R3(18)]
1118	1081	1031	ν[N-C) NO_2+R1(21)]
1036	1002		τ_i[{(H-C-C-C)(CH3-R2+R2)(16)]
1034	1000		τ_i[{(H-C-C-C)(CH3-R2)(21)]
1033	998	998	β [(C-C-C)R1(69)]
1014	981		β [(H-C-C)R1(65)]
997	964	934	τ_i[{(H-C-C-C)(R1)(57)]
952	921		ν_{as}[C-C) CH_3-R4+R4(24)]+τ_i[{(H-C-C-C)(CH_3-R4)(17)]
950	919		τ_i[{(H-C-C-C)(CH_3-R4)(18)]
944	913	910	β [(H-C-C)R1+R2+R3(18)]
904	875	882	τ_i[{(H-C-C-C)(R2)(27)]
892	863		τ_i[{(H-C-C-C)(R1)(43)]
877	848	845	τ_i[{(H-C-C-C)(R1)(95)]
871	842		ν_{as}[(O-C) COOH(17)]
859	830		τ_i[{(H-C-C-C)(R1)(93)]
837	810	811	β [(O-N-C)NO_2(17)]
788	762	776	ν_{as}[(C-C) CH3-R2+R2(16)]
761	736		τ_o[{(O-C-C-C)(R1)+(O-C-O-C)COOH}(40)]
743	719	722	τ_o[(O-C-O-N)(NO_2-R1)(40)]
712	689		τ_o[(O-C-O-N)(NO_2-R1)(19)]
708	684	685	τ_o[(O-C-O-N)(NO_2-R1)(21)]
690	667	667	τ_i[(H-O-C-C)(COOH)(21)]
666	644		τ_i[(H-O-C-C)(COOH)(35)]
642	621		β [(O-N-O)COOH(17)]
640	618		β [(C-C-C)R1+R3(41)]
621	600		β [(O-N-O)COOH(18)]
594	574		β [(O-N-O)COOH(18)]+ τ_i[(H-O-C-C)(COOH)(20)]
576	557		β [(O-C-C)R2+R4(25)]
543	525	5532	τ_i[(H-O-C-C)(COOH)(30)]
539	521		β [(O-N-C)NO_2-R1(26)]
534	516		β [(O-N-C)NO_2-R1(19)]
517	500	459	β [(O-N-C)NO_2-R1(19)]
419	405	415	τ_i[(C-C-C-C)(R1)(53)]
398	385		β [(O-C-C)COOH(16)+(C53-C52-N7)(19)]
390	377		τ_o[(C-C-C-C)(CH_3-R4+R4)(40)]
389	377		τ_o[(C-C-C-C)(CH_3-R2+R2)(40)]
375	363		τ_o[(C-C-C-C)(CH_3-R2+R2)(30)]
272	263		τ_o[(N-C-C-C)(NO_2-R1+R1)(27)]
241	233		τ_i[(H-C-C-C)(CH3-R2+R2)(20)]+ τ_i[(H-C-C-C)(CH3-R4+R4)(16)]
230	222		τ_i[(H-C-C-C)(CH3-R2+R2)(23)]
224	216		τ_i[(H-C-C-C)(CH3-R4+R4)(43)]
175	169		β [(N-C-C)NO_2-R1(22)+(C-C-C)COOH+R1(18)]
106	103		τ_i[{(C-C-C-C)(R2)+(C53-C52-N7-C4)}(22)]
79	77		τ_i[{(C-C-C-C)(R2)+(C53-C52-N7-C4)}(19)]

Frequency, cm^{-1}			Assignment
Cal.	Scaled	Exp. FTIR	
65	63		τ_i[(O-N-C-C)(NO_2-R1)(30)]+ τ_i[(C-C-C-C)(R1+R2+R3-R4)(18)]
62	60		τ_i[(O-C-C-C)(COOH)(35)]
58	56		τ_i[(C-C-C-C)(R1+R2+R3-R4)(20)]
43	41		τ_o[(C52-C4-C8-N7)(34)]
41	40		τ_i[(C-C-C-C)(R1+R2+R3-R4)(19)]
32	33		τ_i[(O-N-C-C)(NO_2-R1)(29)]
31	30		τ_i[(O-C-C-C)(COOH)(24)]
25	25		τ_i[(O-C-C-C)(COOH)(18)]

ν: stretching; ν_s: symmetric stretching; ν_{as}: anti-symmetric stretching; β: bending in-plane; β_O: bending out-of-plane; τ_i: torsion in plane; τ_o: torsion out-of-plane

Table SV. Experimental and calculated absorption wavelengths, excitation energies, absorbance values and oscillator strengths of MTDOSA

Excitation energy, eV	Wavelength, nm		Oscillator strength	Orbital transition
	TD-DFT/B3LYP/ 6-311++G(d,p)	Experimental		
5.5109	224.98	225.6	0.1984	HOMO-4→LUMO+4(5%)
				HOMO→LUMO+6(18%)
				HOMO→LUMO+7(50%)
				HOMO→LUMO+8(6%)
5.4198	228.76		0.0100	HOMO→LUMO+5(36%)
				HOMO→LUMO+6(29%)
				HOMO→LUMO+7(39%)
5.3300	232.61		0.0002	HOMO-4→LUMO+1(68%)
				HOMO-4→LUMO+2(13%)
				HOMO-2→LUMO+1(12%)
4.3627	284.19	288.2	0.0187	HOMO-1→LUMO+1(11%)
				HOMO →LUMO+1(70%)
				HOMO→LUMO+2(09%)
3.5586 eV	348.41		0.1312	HOMO-1 →LUMO(77%)
				HOMO →LUMO(20%)

Table SVI. Experimental and calculated absorption wavelengths, excitation energies, absorbance values and oscillator strengths of NTDOSA

Excitation energy, eV	Wavelength, nm		Oscillator strength	Orbital transition
	TD-DFT/B3LYP/ 6-311++G(d,p)	Experimental		
4.0163	308.70	269.4	0.1391	HOMO-4→LUMO(70%)
				HOMO-3→LUMO(25%)
4.3298	286.35		0.1751	HOMO-5→LUMO(88%)
				HOMO→LUMO+2(7%)
4.4276	280.02		0.0109	HOMO-11→LUMO(34%)
				HOMO-10→LUMO(38%)
				HOMO-3→LUMO+1(15%)
				HOMO →LUMO+2(15%)
4.4376	279.39		0.0502	HOMO-11→LUMO(08%)

				HOMO-10 →LUMO(9%) HOMO-5→LUMO(7%) HOMO -3→LUMO+1(12%) HOMO →LUMO+2(57%)
4.6466	266.83		0.0110	HOMO-3 →LUMO+1(14%) HOMO→LUMO+3(67%) HOMO→LUMO+4(5%) HOMO→LUMO+5(09%)
4.6933	264.17		0.0067	HOMO→LUMO+3(8%) HOMO →LUMO+4(89%)
5.0769	244.21		0.0521	HOMO -4→LUMO+1(26%) HOMO-3 →LUMO+1(06%) HOMO -2→LUMO+2(46%) HOMO-2 →LUMO+3(06%) HOMO-1 →LUMO+1(5%)
5.2619	236.25		0.0717	HOMO-5→LUMO+1(25%) HOMO→LUMO+6(26%) HOMO→LUMO+7(35%)
5.2780	234.91	233.2	0.1370	HOMO-5→LUMO+1(32%) HOMO→LUMO+7(48%)

Table SVII. Experimental and theoretical, ^{1}H and ^{13}C NMR isotropic chemical shifts (with respect to TMS) MTDOSA with DFT (B3LYP/6-311++G(d,p)) method in DMSO.

Atom	$\delta_{cal.}$ / ppm	$\delta_{exp.}$/ ppm	Assignment
		Carbon	
C1	56.5682	40.96	[C(R2)]
C2	42.6899	31.05	[C(R2)]
C3	45.5566	32.27	[C(R2)]
C4	167.2499	115.88	[C(R2,R3)]
C5	126.1185	113.57	[C(R2,R3)]
C6	205.9577	196.62	[C(R2)]
C8	162.6507	115.88	[C(R3,R4)]
C9	127.596	113.57	[C(R3,R4)]
C10	37.2998	50.86	[C(R3)]
C11	46.3124	32.27	[C(R4)]
C12	42.923	31.05	[C(R4)]
C13	56.0562	40.96	[C(R4)]
C14	205.9336	196.62	[C(R4)]
C17	146.5313	129.40	[C(R1)]
C18	138.1241	136.59	[C(R1)]
C19	123.7251	129.40	[C(R1)]
C20	167.5973	158.06	[C(R1)]
C21	114.6153	129.40	[C(R1)]
C22	136.3578	136.59	[C(R1)]
C23	33.6405	27.43	[C(CH_3-R2)]
C24	26.7414	27.43	[C(CH_3-R2)]
C25	33.8613	29.34	[C(CH_3-R4)]
C26	26.8242	29.34	[C(CH_3-R4)]
C28	57.4729	55.21	[C(CH_3-O-R1)]

C57	61.5561	93.52	[C(NR3)]
C58	48.0001	50.86	[C(CH_2)]
C62	177.5777	162.21	[C(COOH)]
C66	176.9226	162.21	[C(COOH)]
		Hydrogen	
Atom	$\delta_{cal.}$ / ppm	$\delta_{exp.}$/ ppm	Assignment
H29	2.1596	2.44(2H, s)	[s, H(R2)]
H30	2.4513	2.44(2H, s)	[s, H(R2)]
H31	2.9517	2.16-2.12(2H, m)	[m, H(R2)]
H32	2.1395	2.16-2.12(2H, m)	[m, H(R2)]
H33	5.3505	4.78(br s)	[s, H(C-R1,R3)]
H34	2.6412	2.23-2.19(2H, m)	[m, H(R4)]
H35	1.8643	2.23-2.19(2H, m)	[m, H(R4)]
H36	2.1917	2.44(2H, s)	[s, H(R4)]
H37	2.0298	2.44(2H, s)	[s, H(R4)]
H38	7.8589	7.17(1H, *d*, *J* = 8.8 Hz)	[d, H(R1)]
H39	6.9039	6.73(1H, *d*, *J* = 8.4 Hz)	[d, H(R1)]
H40	6.8884	6.73 (1H, *d*, *J* = 8.4 Hz)	[d, H(R1)]
H41	8.1223	7.17 (1H, *d*, *J* = 8.8 Hz)	[d, H(R1)]
H42	1.1034	0.97 (3H, s)	[s, H(CH_3-R2)]
H43	1.1004	0.97 (3H, s)	[s, H(CH_3-R2)]
H44	1.1731	0.97 (3H, s)	[s, H(CH_3-R2)]
H45	1.3565	0.97 (3H, s)	[s, H(CH_3-R2)]
H46	0.8171	0.97 (3H, s)	[s, H(CH_3-R2)]
H47	0.8885	0.97 (3H, s)	[s, H(CH_3-R2)]
H48	0.9945	1.08 (3H, s)	[s, H(CH_3-R4)]
H49	1.0912	1.08 (3H, s)	[s, H(CH_3-R4)]
H50	1.1789	1.08 (3H, s)	[s, H(CH_3-R4)]
H51	0.8115	1.08 (3H, s)	[s, H(CH_3-R4)]
H52	1.3637	1.08 (3H, s)	[s, H(CH_3-R4)]
H53	0.8535	1.08 (3H, s)	[s, H(CH_3-R4)]
H54	4.1108	3.71 (3H, s)	[s, H(CH_3-O-R1)]
H55	3.7625	3.71 (3H, s)	[s, H(CH_3-O-R1)]
H56	3.7903	3.71 (3H, s)	[s, H(CH_3-O-R1)]
H59	4.7417	4.78	[H(C-R3)]
H60	3.752	4.67	[H(CH_2)]
H61	2.8325	4.67	[H(CH_2)]
H65	9.7824		[H(COOH)]
H69	6.9706		[H(COOH)]

Table SVIII. Experimental and theoretical, ^{1}H and ^{13}C NMR isotropic chemical shifts(with respect to TMS) of NTDOSAwith DFT (B3LYP/6-311++G(d,p)) method in DMSO

Atom	$\delta_{cal.}$ / ppm	$\delta_{exp.}$/ ppm	Assignment
		Corbon	
C1	55.8721	53.92	[C(R2)]
C2	42.4765	39.38	[C(R2)]
C3	45.4334	42.72	[C(R2)]
C4	168.7219	164.52	[C(R2,R3)]
C5	125.0398	91.07	[C(R2,R3)]
C6	205.9295	182.18	[C(R2)]
C8	164.4064	151.97	[C(R3,R4)]
C9	125.6429	96.80	[C(R3,R4)]
C10	39.3279	39.17	[C(R3)]
C11	46.4148	42.72	[C(R4)]
C12	42.9173	42.51	[C(R4)]
C13	55.6659	52.71	[C(R4)]
C14	206.2335	182.51	[C(R4)]
C17	164.7724	144.22	[C(R1)]
C18	138.2502	130.00	[C(R1)]
C19	130.0735	107.60	[C(R1)]
C20	156.7579	142.48	[C(R1)]
C21	131.4079	111.25	[C(R1)]
C22	136.0572	114.92	[C(R1)]
C23	33.4636	38.28	[C(CH_3-R2)]
C24	26.7644	27.03	[C(CH_3-R2)]
C25	33.1922	38.07	[C(CH_3-R4)]
C26	26.7744	27.93	[C(CH_3-R4)]
C52	61.8097	72.18	[C(NR3)]
C53	47.6303	44.03	[C(CH_2)]
C57	177.6375	179.68	[C(COOH)]
C61	176.4971	177.84	[C(COOH)]
		Hydrogen	
H27	2.2047	2.69-2.59 (2H, m)	[m, H(R2)]
H28	2.419	2.69-2.59 (2H, m)	[m, H(R2)]
H29	2.9088	2.69-2.59 (2H, m)	[m, H(R2)]
H30	2.1713	2.69-2.59 (2H, m)	[m, H(R2)]
H31	5.5051	4.51 (s)	[s, H(R3)]
H32	2.6342	2.69-2.59 (2H, m)	[m, H(R4)]
H33	1.9143	2.69-2.59 (2H, m)	[m, H(R4)]
H34	2.2446	2.69-2.59 (2H, m)	[m, H(R4)]
H35	2.1475	2.69-2.59 (2H, m)	[m, H(R4)]
H36	8.0988	6.76 (1H, *d*, *J* = 8.8 Hz)	[d, H(R1)]
H37	8.1757	7.07 (1H, *d*, *J* = 8.4 Hz)	[d, H(R1)]
H38	8.4868	7.07 (1H, *d*, *J* = 8.4 Hz)	[d, H(R1)]
H39	8.4312	6.76 (1H, *d*, *J* = 8.8 Hz)	[d, H(R1)]
H40	1.1063	1.83 (3H, s)	[s, H(CH_3-R2)]
H41	1.119	1.83 (3H, s)	[s, H(CH_3-R2)]

Atom	$\delta_{cal.}$ / ppm	$\delta_{exp.}$/ ppm	Assignment
H42	1.2112	1.83 (3H, s)	[s, H(CH_3-R2)]
H43	1.3445	1.23 (3H, s)	[s, H(CH_3-R2)]
H44	0.8175	1.23 (3H, s)	[s, H(CH_3-R2)]
H45	0.895	1.23 (3H, s)	[s, H(CH_3-R2)]
H46	0.9771	2.25 (3H, s)	[s, H(CH_3-R4)]
H47	1.071	2.25 (3H, s)	[s, H(CH_3-R4)]
H48	1.1639	2.25 (3H, s)	[s, H(CH_3-R4)]
H49	0.8346	1.94 (3H, s)	[s, H(CH_3-R4)]
H50	1.3659	1.94 (3H, s)	[s, H(CH_3-R4)]
H51	0.8936	1.94 (3H, s)	[s, H(CH_3-R4)]
H54	4.7507	2.34-2.33 (1H, m)	[s, H(C-R3)]
H55	3.801	2.33-2.28 (2H, m)	[m, H(CH_2)]
H56	2.8027	2.33-2.28 (2H, m)	[m, H(CH_2)]
H60	9.8863		[H(COOH)]
H64	6.9745		[H(COOH)]